8-2020

Experimental Study of the Alteration of Basalt on the Surface of Venus

Hannah Teffeteller
University of Tennessee, Knoxville, hteffete@vols.utk.edu

To the Graduate Council:

I am submitting herewith a thesis written by Hannah Teffeteller entitled "Experimental Study of the Alteration of Basalt on the Surface of Venus." I have examined the final electronic copy of this thesis for form and content and recommend that it be accepted in partial fulfillment of the requirements for the degree of Master of Science, with a major in Geology.

Dr. Molly McCanta, Major Professor

We have read this thesis and recommend its acceptance:

Dr. Molly McCanta, Dr. Nicholas Dygert, Dr. Micah Jessup

Accepted for the Council:
Dixie L. Thompson

Vice Provost and Dean of the Graduate School

(Original signatures are on file with official student records.)

Experimental Study of the Alteration of Basalt on the Surface of Venus

A Thesis Presented for the

Master of Science

Degree

The University of Tennessee, Knoxville

Hannah Teffeteller

August 2020

Abstract

Venus is the second planet from the sun, distinguished by its thick atmosphere which prevents visible observations of the surface. Our understanding of its surface is therefore dominated by surface interactions with electromagnetic radiation (e.g. radar, visible-to-infrared, and X-ray wavelengths) which have been collected by a series of missions including the Soviet's Venera missions, the National Aeronautics and Space Administration's (NASA) Magellan mission, and the European Space Agency's (ESA) Venus Express orbiter (Barsukov et al. 1982; Head et al. 1992; Smrekar et al. 2010). The atmosphere of Venus is composed almost entirely (~97%) of CO_2 gas with trace amounts of SO_2 gas (~150ppmv) (Zolotov 2018). The surface of Venus experiences temperatures of ~470˚C and pressures of ~92 bars, comparable to the terrestrial greenschist metamorphic facies, which has been used to suggest that rocks on the surface could interact with their atmosphere (Urey 1952, Lewis 1970, Barsukov et al. 1982; Fegley and Treiman 1992, Zolotov 2018). Most of the surface of Venus is covered by basaltic plains and volcanoes assumed to have been emplaced ~300–600 Ma (Nimmo and McKenzie 1998). However, several authors have proposed volcanism is currently active or has been within the last hundreds of thousands of years based on variations in thermal emissivity spectra and recent basalt and mineral oxidation experiments (Head et al. 1992; Smrekar et al. 2010; Stofan et al. 2016; D'Inecco et al. 2017; Filiberto et al. 2020). Should basaltic rock interact with the Venusian atmosphere, interpretations of spectral data rely on an understanding of the alteration products and their rates of formation. We used an experimental approach to model how basaltic glass interacts with a Venus-like atmosphere and quantified the changes in geochemical composition of the sample surfaces and at depth. Our results confirm that iron (Fe) oxides can form on the surfaces of basalts under Venus surface conditions in two weeks duration. Moreover,

our results corroborate the findings of Cooper et al. (1996) that cation diffusion is the rate-limiting factor for basalt alteration and constrain the ages of basalts on Venus to be anywhere from 268 – 1,900 years old.

Table of Contents

List of Tables

List of Figures

Section 1: Introduction

The surface of Venus is believed to be composed primarily of basalt, in the form of volcanic plains, shield volcanos and other volcanic constructs, that represent igneous activity assumed to have taken place during Venus' major resurfacing event of 300-600 Ma ago (Head et al. 1992; Nimmo and McKenzie 1998). Material on the surface of Venus experiences temperatures of ~470ºC and pressures of ~90 bars, comparable to the terrestrial greenschist metamorphic facies (Barsukov, Volkov, and Khodakovsky 1982; Fegley and Treiman 1992). In contrast to the Earth, the atmosphere of Venus is 96.5% carbon dioxide (CO_2) with trace amounts of sulfur dioxide (SO_2) and other gas species (Zolotov 2018,Table 1). The oxidation state (quantified as oxygen fugacity, or fO_2) of the near surface-atmosphere of Venus is near the magnetite-hematite (M-H) buffer, which has been used to suggest that the basalts on the surface may be covered by either or both species of iron (Fe) oxides (Figure 1). New interpretations of spectral data of the surface as well as recent experimental basalt weathering data suggests that the planet could still be volcanically active based on the speculated presence of iron (Fe) oxides on some older volcanic plains, the lack thereof on their volcanic centers, and the overall red hue observed on the surface (Figures 2,3) (Pieters et al. 1986; Smrekar et al. 2010; Stofan et al. 2016; D'Incecco et al. 2017; Filiberto et al. 2020). Several authors have suggested that volcanism is presently active on the surface of Venus, citing high thermal emissivity values as evidence for recent lava flows based on temperature (Hashimoto et al. 2008; Shalygin et al. 2015). However, thermal emissivity is not a direct measurement of surface temperature alone and can be affected by factors such as grain size and mineralogy. If volcanic activity were occurring in the last several thousand years, this would challenge the long-standing major resurfacing event hypothesis.

Previous work on the oxidation of basalt glasses under terrestrial atmospheric compositions (i.e., in the presence of H_2O) at temperatures greater than 550˚C suggests that Ca^{2+}, Fe^{2+}, and Mg^{2+} cations will migrate to the surface to form oxides (Cook et al. 1990; Cooper et al. 1996; Berger et al. 2019). Similarly, oxidation reactions at high temperatures have been studied for ferromagnesian silicate materials that demonstrate the ability to produce surface coatings of iron oxides (Fe_xO) and various sulfur-bearing phases, such as anhydrite ($CaSO_4$) and minor pyrite (FeS_2) (Fegley et al. 1995a; Filiberto et al. 2020). However, studies of basalt oxidation and ferromagnesian silicate oxidation have been conducted under terrestrial atmospheric conditions in the presence of abundant H_2O, making it is unclear how applicable their results are to the anhydrous surface-atmosphere system of Venus.

An understanding of the rock compositions at the surface of Venus and their potential chemical weathering, or alteration, products is important for interpretation of both the spectral and *in-situ* data collected during previous missions as well as informing future missions. Identifying primary crustal composition, a goal of any future mission, may be difficult if alteration products are prevalent. Additionally, if primary basaltic material erupted onto the surface is obscured by chemical weathering processes, understanding the alteration products and their associated timescales of formation may provide a way to age date specific volcanic flows. Future missions that work to characterize the geochemistry at the surface of Venus will therefore rely on an understanding of how basaltic rock at the surface interacts with the atmosphere.

The experiments presented here will allow for characterization of basalt glass alteration products formed under Venus surface conditions. The hypotheses to be tested will include: 1) oxides will form on the surfaces of basalts during experimental runs due to oxidizing conditions; 2) the thickness of the alteration products will increase with the square root of time; 3) different

starting compositions will weather in different manners with production of different alteration products. Understanding the products, processes, and rates of chemical weathering of basalt on Venus will allow us to understand what geochemical analyses are expected on the surface (either via *in-situ* analyses or spectral analyses), how distinct they should be based on the rate(s) of their formation, the age of the lava flows on the surface, and how the igneous diversity at the surface might or might not be obscured via weathering processes.

Section 2: Background

2.1 The surface of Venus

Although Venus and Earth are neighboring planets with similar masses, densities, and proximities to the sun, the composition of their atmospheres and the appearances of their surfaces differ dramatically. One of the first differences observed for Venus was the atmospheric temperature and pressure at the surface, which have now been estimated to be ~470ºC and 90 bars, respectively (Barsukov et al. 1982). Venus' optically thick and opaque atmosphere prevents any type of visual observation of the surface and limits spectral observations, obscuring the study of both the atmosphere and surface. Nevertheless, Venera 11/12 and Pioneer Venus spacecraft were able to collect *in-situ* measurements of the near surface atmosphere which yielded $CO:CO_2$ concentrations in agreement with those predicted in the near surface based on IR spectroscopy measurements, within error (Lewis and Kreimendahl 1980). The $CO:CO_2$ ratio predicted that the oxidation state of the atmosphere (or fO_2) was at or above the M-H buffer for the near surface (Lewis and Kreimendahl 1980; B. Fegley et al. 1995). The M-H buffer is significantly more oxidizing, for example, than the oxidation state at which most terrestrial basalts are formed, approximated to be around the quartz-fayalite-magnetite (QFM) buffer (Figure 1). Because the atmosphere of Venus is predicted to be at or near the M-H buffer, several authors have suggested that magnetite and/or hematite are present on the surfaces of basalts and act to buffer the atmosphere (Fegley et al. 1995; Fegley et al. 1997). The visible red hue on the surface observed at the Venera 13 site (Figure 2) was used to suggest that hematite coats the surfaces of basalts (Pieters et al. 1986), while near-IR emissivity anomalies measured by the VIRTIS spectrometer on Venus Express (Figure 3) have been used as evidence for the presence of Fe oxide(s) (Smrekar et al. 2010).

Lander missions provide geochemical data on the surface composition; however, designing landers to withstand the high temperatures and pressures at the surface is technologically difficult. Under the harsh atmospheric conditions at the surface, electronics that rely on silicon semiconductors can only function for several hours before dying even when encapsulated inside protective vessels (Neudeck et al. 2016). Despite the technological difficulties, a series of successful Soviet lander and orbiter missions (Venera and VEGA) in the 1970s and 1980s were able to collect *in*-situ compositional data for the surface of the planet. Seven sites were analyzed; however, only three sites included analyses for major element bulk chemistry: Venera 13, 14, and VEGA 2 (Surkov and Barsukov 1985, Surkov et al. 1986). These three sites were focused on either lava plains or rises, whose basaltic rock compositions were inferred based on *in-situ* X-ray fluorescence (XRF) analyses at these sites. Venera 13 landed on a volcanic rise and its analyses were analogous to an alkali basalt while Venera 14 and VEGA 2 were centered on volcanic plains and their analyses were consistent with a tholeiitic mid-ocean ridge basalt (Table 2) (Basilevsky et al. 2007, Filiberto 2014). The range of geochemical composition observed at the surface as well as the diversity in geomorphological features such as volcanic plains, shield volcanoes, and the Ishtar Terra highland suggests a potentially diverse magmatic history for a planet currently lacking Earth-style plate tectonics.

2.2 Thermodynamic equilibrium modeling of rock-atmosphere interaction

Although *in-situ* geochemical data was collected at the surface, the error associated with the measurements far exceeds accepted error in terrestrial and Mars Exploration Rover (MER) and Mars Science Laboratory (MSL) rover analyses. Despite the low precision of the surface data, several authors have modeled the chemical weathering process(es) assuming equilibrium between basaltic rock and the oxidizing atmosphere of Venus (Barsukov et al. 1982; Treiman

and Schwenzer 2009). These models show that network modifying cations such as Ca^{2+} and Fe^{2+} in basalt glass should react at the surface to form secondary alteration phases such as anhydrite ($CaSO_4$) and iron (Fe) oxides (magnetite or Fe_3O_4, hematite or Fe_2O_3), leaving a residue rich in Al and Si that equilibrates to anhydrous cordierite + enstatite + quartz . Thermodynamic equilibrium calculations of Fe oxide stability with respect to Venus' CO_2 concentration show how Fe^{2+} in silicates may be oxidized:

$$3FeO\ (\text{in silicates}) + CO_2 \rightarrow Fe_3O_4\ (\text{magnetite}) + CO\ (g) \qquad \text{Eq. 1}$$

Magnetite may be partially oxidized further to form hematite via the reaction (Zolotov 2018):

$$2Fe_3O_4 + CO_2 \rightarrow 3Fe_2O_3\ (\text{hematite}) + CO\ (g) \qquad \text{Eq. 2}$$

The rate at which secondary minerals such as iron oxide could form within the Venus atmosphere remains unconstrained, however understanding the formation rates of such minerals due to surface-atmosphere interaction would result in age estimates for basalts coated in magnetite and/or hematite. Weathering of basalt to form anhydrite, cordierite, and quartz could cause a significant mass and volume increase that may explain the platy texture observed on the surface from lander missions (Treiman and Schwenzer 2009). Furthermore, the presence of anhydrite and/or Fe oxide on glassy basalts should be detectable in thermal emissivity analyses of the surface like those returned from the European Space Agency's Venus Express orbiter. However, S/Ca ratios of Venusian soils imply that the formation of anhydrite did not go to completion (Fegley and Treiman 1992).

2.3 Experimental modeling of rock-atmosphere interaction

While thermodynamic equilibrium modeling increased our understanding of the potential reactions occurring at the surface of Venus, constraints on the kinetics of formation of secondary minerals were needed to better constrain chemical weathering of basalt. One experimental study investigated the interaction between basalt rock and terrestrial atmosphere (1 bar pressure, in the

presence of H_2O) and found that at temperatures of 500-600ºC secondary phases of crystalline CaO and MgO were formed on the surface of basalts. Analysis of the samples following experimentation demonstrated the development of a reaction zone, characterized by a depletion of Ca^{2+} and Mg^{2+} and enrichment of Na^{+} (Cooper et al. 1996). The reaction zone morphology was directly related to the style of oxidation, where cations with a 2+ charge diffusively migrated to the free surface, thereby increasing the oxygen/cation ratio (i.e. oxidation state) within the basalt glass. The flux of Na^{+} from depth to the oxidized zone, depleted in divalent cations, was thermodynamically favorable and acted to stabilize Fe^{3+} as a network former. Oxidation was thus induced by creating an oxidation potential, where the oxidation state of the atmosphere during experimentation (near the quartz-fayalite-magnetite, or QFM, buffer) was substantially greater than the oxidation state of basalt glass during formation (just above the quartz-iron-fayalite, or QIF, buffer). Therefore, oxidation was driven by the diffusion of network modifying cations (i.e. divalent species Ca^{2+}, Fe^{2+}, and Mg^{2+}) and was consequently the rate-limiting factor to basalt glass alteration. Assuming layers of crystalline secondary phases form as slabs on the free surfaces of basalts, their growth rate follows parabolic kinetics and should increase with the square root of time (Cook et al. 1990; Cooper et al. 1996). The findings of this study would allow for age dating of specific basalt flows, assuming Fe oxides are present. However, the study investigated basalt oxidation under the presence of H_2O and at a lower fO_2 than that estimated for the surface of Venus, making it unclear how applicable the results are.

A recent experimental study of chemical weathering of basalt investigated the reaction between rock and atmosphere using olivine, assumed to be a major component of basalt (Filiberto et al. 2020). These experiments show that nanoscale secondary phases of hematite are formed within hours on centimeter-sized grains reacted under terrestrial atmospheric conditions

(i.e., in the presence of H_2O) at 1 atm and at temperatures of 600ºC and 900ºC (Filiberto et al. 2020). A similar study investigating the weathering of pyroxene grains, another major component of basalt, at a temperature of 600ºC and terrestrial atmospheric conditions (i.e. in the presence of H_2O) at 1 atm found that hematite formed on the surface of pyroxene grains, albeit an order of magnitude slower than olivine (Cutler et al. 2020). The same study also found that oxidation of basalt obscured nearly all olivine and/or pyroxene spectral signatures. This result is consistent with data from Venera 9 and 10 landers where images of the basaltic surface were characterized by a red hue (Pieters et al. 1986).

Another recent experimental study investigated basaltic rock and glass alteration by subjecting both olivine and basalt glass samples to Venus-like atmospheres (some dry and some water-bearing, to simulate early Venus) under appropriate Venus surface temperatures (475ºC), pressures (~90 bars), and oxygen fugacity conditions (near the Ni-NiO buffer) for several days (Berger et al. 2019). Both olivine and basalt glass subjected to dry gas (a mixture of CO_2, N_2, and SO_2) formed thin coatings of Fe oxide and sulfates ($(Ca,Na)SO_4$), where the specific phase of Fe oxide was not confirmed. The applicability of these results to the surface of Venus is complicated by use of significantly lower oxygen fugacity (near the Ni-NiO buffer) in experimentation than that assumed to exist at the surface (near the M-H buffer) (Figure 1).

2.4 Effects of rock-atmosphere interaction on spectral data

The production of secondary phases on basalts at the surface could have direct implications for spectral analyses. Weathering of basalt on Venus may produce an optically thick (μm to mm) rind that is different in chemical composition and structure compared to basalt, as observed on terrestrial basalts (McCanta et al. 2015). A secondary phase such as Fe-oxide would produce lower thermal emissivity spectra than a fresh, unweathered basalt (Gilmore et al. 2017).

Thermal emissivity data has been collected by the VIRTIS spectrometer on the European Space Agency's Venus Express spacecraft in the atmospheric window at 1.02μm and produced spectral analyses from the top few micrometers (μm) of the surface (Smrekar et al. 2010). The increased thermal emissivity of surfaces observed near volcanic centers (Figure 3) was contrasted with the lower thermal emissivity observed at the basaltic plains to suggest that older basalts were coated by Fe oxides and that volcanism is still active today (Smrekar et al. 2010; Filiberto et al. 2020). Filiberto et al. (2020) described the effect of oxidation on the visible to near-infrared (VNIR) spectra of olivine, observing a dramatic increase in the production of Fe oxide with time at 600ºC. As alteration duration increased, reflectance spectra became increasingly flat and were interpreted to represent the formation of magnetite (Filiberto et al. 2020). Alteration under even greater temperatures (900ºC) developed spectral features characteristic of hematite after one month of oxidation (Filiberto et al. 2020). Therefore, it was suggested that magnetite forms on the surfaces of basalts as a result of oxidation and is then converted to hematite with increasing time (Filiberto et al. 2020). While thermodynamically hematite and/or magnetite are expected to form on the surface of Venus, their coexistence and rates of formation are still not well constrained.

Section 3: Methods

3.1 Experimental set-up

A series of high-pressure alteration experiments on basaltic glasses were conducted in cold-seal pressure vessels at Brown University. Two starting compositions were used: a natural alkaline basalt from Sverrefjell volcano, Svalbard (Skjelkvale et al. 1989) which is chemically similar to Venera 13 rock (A. H. Treiman 2007); and a synthetic tholeiite basalt based on the Venera 14 rock analyses (A. H. Treiman 2007) with assumptions made regarding those elements not analyzed (Table 2)(Filiberto 2014). These compositions were chosen based on the diversity of basaltic rock analyzed on the surface of Venus by Venera and VEGA lander missions. The tholeiitic composition represents Venus 'plains' basalts, while the alkaline basalt represents Venus' 'plume' basalts. The synthetic tholeiitic basaltic glass was fused from oxides at 1 atm, 1300ºC, and fO_2 at the QFM buffer. The tholeiitic basalt glass broke to yield relatively flat surfaces and was not treated further before input into the cold-seal pressure vessel. Samples of natural alkaline basalt were cut into 1 mm-thick slabs and polished prior to reaction. Glassy samples were chosen because glass is likely to be more susceptible to alteration than minerals. Moreover, previous experimental studies confirm that glassy basaltic products should be present on the surface of Venus as the surface temperature is lower than that of basalt magma (~1100ºC) and the glass transition temperature for basaltic compositions (~750ºC) (Bender *et al.*, 1978; Ryan and Sammis 1981; Cooper *et al.*, 1996).

Experimental temperature conditions included two temperatures, either 470ºC or 700ºC, at a pressure of ~90-92 bars to simulate surface conditions on Venus (470˚C). The 700˚C condition was selected to advance the rate of weathering reactions while staying under the glass transition temperature. Samples were contained in gold tubing and placed into cold-seal bombs (Figure 4). To simulate Venus atmosphere conditions, the apparatus was pressurized using pure CO_2 gas.

Samples were run for two-week durations, extending the experimentation time to four weeks for one tholeiitic sample VEN-7B in order to isolate the effect of time on alteration (Table 3). Runs VEN-4 (A,B) and VEN-5 (A,B) included a hematite-magnetite (H-M) solid buffer to raise the fO_2 of the experiment to values consistent with that of the Venus surface (Zolotov 2018); all others were buffered only with CO_2 resulting in reducing conditions near the GCO (graphite-CO) buffer (Table 3).

3.2 Sample preparation

The focused ion beam (or FIB) *in-situ* lift-out technique is a process by which a thin foil cross section can be extracted from a geologic sample, allowing for characterization of a sample's surface and below its surface. This process is particularly useful for preparing a sample for chemical and/or structural micro-scale analyses using the transmission electron microscope (or TEM) which requires a thin sample, usually around 100 nanometers (nm) in thickness. Samples were prepared for TEM analyses using the dual-beam FEI Quanta 3D FEG instrument at Johnson Space Center (JSC).

Once a sampling location was identified, a thin layer (~0.8-1.0 μm) of carbon was deposited over the sample area using an electron beam operating at 5.0 kV and 3.4 nA; this layer, often referred to as "e-beam carbon", had a length of ~20 μm and a width of 1.5 μm which helped protect the surface from damage that could be incurred from the ion beam. While not always a part of the FIB *in-situ* lift-out technique, this step was especially important for samples whose surface chemistry was important to preserve. Following e-beam carbon deposition, another layer of carbon was deposited over the sample area. This layer was deposited using the ion-beam, referred to as "i-beam carbon", and was thicker (~ 3.5 μm) and wider than the e-beam carbon layer, having dimensions of ~30 μm x 2.5 μm x 3.5 μm (Figure 5). Beam conditions for

the ion beam carbon deposition were 30 kV and 0.10 nA. This region of carbon was referred to as the “cap” since it forms a topographically distinct cover over the sample area and served to further protect the sample surface during subsequent ion-bombardment or milling (Figure 5).

Once the protective cap was deposited, the milling process began. Two rectangular boundaries (measuring approximately 32 μm x 16 μm x 3.5 μm) were superimposed on the image of the sample’s surface. Material in these areas was milled away using a gallium (Ga) ion beam operating at 30 kV and 15 nA. These features are often referred to as “trenches” and allow more milling to be done at depth in the sample (Figure 6). Once the trenches were milled, side and under cuts were milled away to further isolate the section from the rest of the sample body. Only a thin bridge of material remained connecting the section and the sample after the side and under cuts were completed. This material was cut away after a manipulator needle was attached for lift-out. The needle was inserted into the chamber and lowered into a position very close to the section. Platinum (Pt) was used to weld the tip of the needle to the section, and then the bridge of material holding the section to the sample was cut away. The needle was lifted out with the sample attached to it and moved to a TEM grid within the chamber. Together, they were lowered, and the sample was placed very close to the grid. It was welded to the grid using platinum (Pt) and then the connection between the needle and the section was milled away so that the needle could be removed. The section was attached to the grid which was later inserted into the TEM for further analyses. However, before doing so, the section was thinned from ~ 3 μm in width to ~ 80–120 nm for TEM analyses. To thin the section to the desired width, both sides were milled using successively smaller beam current, effectively polishing down the sample until the desired thickness was reached. This sample preparation was used for all samples to obtain chemical analyses and characterize samples on the nanometer scale.

3.3 Analytical characterization using electron probe microanalysis

The geochemistry of the synthetic tholeiite basalt glass and the natural alkaline basalt glass were characterized prior to experimentation at the University of Tennessee using the Phenom Pro scanning electron microscope (SEM) and the Cameca SX-100 electron probe micro-analyzer (EPMA). Operating beam column conditions for analyses of both glasses were 15 keV and 10 nA with a spot size of 15 μm. Ten to fifteen spots of glass were chosen for each starting composition and their averages were taken (Table 4). For the natural alkaline basalt glass, ten spots were measured for each mineral phase present.

3.4 Analytical characterization using Rutherford Backscatter Spectroscopy

The largest fragments from each sample type were sent to Rensselaer Polytechnic Institute for Rutherford Backscatter Spectroscopy (RBS) analysis before and after experimentation (Figure 7). Spectra were generated by focusing a beam of light energetic ions (in this case, He) at specific energies ranging from 3.05 to 3.5 MeV at an angle incident to the sample surface. The energies of the backscattered ions were measured by a detector positioned at an angle of 167 degrees with respect to the incident beam. Collision with the sample surface caused the He ions to scatter and their backscatter energies were measured, where energies were dependent on the masses of the target atoms in the sample with higher backscatter energies related to heavier target atoms. Incident He ions can penetrate several microns (μm) into the sample surface and are thus recording alteration of the surface of the sample. Spectra were collected from relatively flat surfaces on samples following experimentation using a 1 mm^2 spot size. The resulting analyses were in the form of counts and channels, where counts were proportional to concentration and channels were proportional to the related backscatter energy.

The spectra generated from these analyses are plotted as red symbols while the simulated spectra based on the composition of the unreacted basalts is plotted as a blue line.

3.5 Analytical characterization using transmission electron microscopy

Sample chemistry was analyzed using the JEM-2500SE transmission electron microscope (TEM) at NASA's Johnson Space Center (JSC) following appropriate sample preparation as described above. Samples were first characterized on the micron scale using energy dispersive X-ray (EDS) analysis that yielded qualitative chemical analyses (i.e. a measure of x-ray counts for each element) over a specified mapping area. This type of analysis was useful for selecting a sample region, if any, that had been altered. Samples were then characterized using EDS analysis that yielded quantitative chemical analysis (i.e. weight percent for each element) for a line transect within a specified mapping area. This type of analysis was used to characterize the movement of cations throughout the sample's reaction zone following experimentation as well as identifying secondary mineral phases present on the surface. Weight percent analysis can be obtained from EDS line transects on thin foils using the Cliff-Lorimer method whereby characteristic X-ray intensities are converted to concentrations following the equation (3):

$$\frac{C_A}{C_B} = k \cdot \frac{I_A}{I_B} \qquad \text{eq. (3)}$$

where C_A and C_B are concentrations of element A and element B, I_A and I_B are the measured intensities of element A and element B, and k is a proportionality factor determined using standards of selected elements (Cliff and Lorimer 1985). Samples that contained crystalline phases on or near their surfaces were analyzed using the TEM's selected area electron diffraction (SAED) mode whereby a mineral's crystalline structure can be deduced from a diffraction pattern. This is especially useful for grains that are several hundred nanometers to several

microns in diameter whose chemical composition cannot be obtained from a more common method such as SEM EDS. Average compositions for the entire FIB section, from sample surface to several hundred nanometers in the sample interior, for each reacted sample are listed in weight percent (wt %) in table 5. Reacted samples that developed a reaction zone have their reaction zone compositions, in weight percent (wt%), listed in table 6.

Section 4: Results

4.1 Starting basalt compositions

Bulk chemistry of the natural alkaline basalt glass was calculated using estimated modal abundances and average chemical composition of minerals and glass, while bulk chemistry of the synthetic tholeiite basalt glass was determined from analyses of glass alone (Table 4). The natural alkaline basalt glass contained microlites and microphenocrysts of forsterite ($Fo_{85}Fa_{15}$), augite ($(Ca_{0.5}Mg_{0.4}Fe_{0.1})(Al_{0.15}Si_{0.85})_2O_6$), labradorite ($(Ca_{0.6}Na_{0.4})(Si_{0.6}Al_{0.4})_4O_8$), and rare chromite. The estimated modal abundances of each phase were as follows: glass (47%), olivine (20%), pyroxene (20%), plagioclase (12%), and chromite (1%). Following the experiments, samples were characterized by surface texture and/or alteration products using SEM backscatter electron (BSE) images.

4.2 Tholeiite basalts

Low fO2 (Graphite-carbon monoxide buffer, more reducing than Venus surface conditions), 14 days

The Venus surface temperature (470ºC) sample VEN-1 had an overall holohyaline texture with some streaks of non-glassy, secondary phase randomly occurring on the surface. SEM backscatter imaging revealed two secondary phases randomly oriented on the surface that appeared to be an Fe metal phase and a carbon-rich phase, such as graphite (Figure 8). TEM EDS analysis of the glassy region showed no apparent reaction front (Figure 9) which agreed with RBS analysis of the sample that suggested no significant alteration (Figure 7).

The high temperature (700ºC) sample VEN-3 had an overall holohyaline texture with some streaks of non-glassy, secondary phases randomly occurring on the surface. SEM backscatter imaging revealed two secondary phases randomly oriented on the surface that appeared to be an Fe metal phase and a carbon-rich phase, such as graphite (Figure 8). TEM

EDS analysis revealed a zone of reaction extending ~15 nm into the sample from the surface (Figure 10). The reaction zone was subdivided into two different regions, region B and region C, which were distinguishable in geochemistry. The surface layer alteration, or region C, extended from the surface of the sample to a depth of ~5 nm and was characterized by a depletion of Fe by ~4 wt%, Mg by ~5 wt% and an enrichment of Al by ~1 wt% and Si by ~2 wt% when compared to the composition of the unaltered tholeiitic basalt glass (Table 6). Region B extended ~5 nm into the sample body from region C and was characterized by a depletion of Ca by ~2 wt%, Fe by ~5 wt%, Mg by ~5 wt%, and an enrichment of Al by ~1 wt% and Si by ~6 wt% when compared to the unaltered basalt glass (Table 6). The average weight percent concentration of Ca, Na, Mg, and Fe cations for the entire TEM FIB section (~ 185 nm) were depleted as compared to the initial concentrations found in the basalt glass before experimentation (Figure 10). RBS analysis for the section suggested no significant alteration (Figure 7).

High fO2 (Magnetite-hematite buffer, approximates Venus surface condition), 14 days

The Venus surface temperature (470ºC) sample VEN-5B had an overall holohyaline texture with some streaks of surficial, non-glassy Fe, Cr metal and a nano-scale secondary phase that was randomly distributed across the surface (Figure 8). The non-metal phase formed small clumps that ranged in size from several nanometers to several microns. Composition of this secondary phase was not determined using SEM analysis alone due to the small grain size. TEM EDS analysis of the small grains showed that they are Fe rich however quantitative measurements were not acquired for the grains. Their composition can be inferred based on qualitative measurements (i.e. net counts) which was like those from section VEN-4B where the grains were confirmed to be magnetite. TEM EDS analysis revealed a surface layer measuring ~8 nm in depth that was characterized by an enrichment in Ca by ~5 wt%, Fe by ~2 wt%, Mg by

~0.5 wt%, and a depletion in Al by ~2 wt% and Si by ~7 wt% (Table 6; region C, Figure 11). Just below this, another region of alteration (region B, Figure 11) extended ~8 nm and was characterized by a depletion in Ca by ~2 wt%, Fe by ~2 wt%, Mg by ~2%, and an enrichment in Si by ~5 wt% (Table 6). These regions together formed the entire reaction zone of the sample, which measured ~16 nm in depth (Figure 11). The entire reaction zone was characterized by an enrichment of Ca by ~ 1 wt%, and Fe by ~ 0.5 wt%. This agreed with RBS analysis which showed an enrichment of Fe in the near surface of the sample (Figure 7).

The high temperature sample (700ºC) VEN-4B had an overall holohyaline texture with some streaks of surficial, non-glassy metal and a surficial, nano-scale secondary phase that was randomly distributed across the surface (Figure 8). The non-metal phase formed small clumps that ranged in size from several nanometers to several microns. Composition of the secondary phase was not determined using SEM analyses alone because of the small grain size. One cluster of grains that measured ~2 μm in diameter was included in the FIB section to determine the mineralogy of this secondary phase. TEM EDS and SAED analyses confirmed that the phase was magnetite (Fe_3O_4). TEM EDS analysis revealed a surface layer measuring ~7 nm in depth that was characterized by an enrichment in Ca by ~5 wt%, Fe by ~1 wt%, and by a depletion in Al by ~3 wt%, Mg by ~4 wt%, and Si by ~1 wt% (Table 6; region C, Figure 12). Below region C was region B which extended to a depth of ~ 16nm and was characterized by a depletion of Ca by ~4 wt%, Fe by ~4 wt%, Mg by ~4 wt%, and an enrichment in Si by ~20 wt% (Table 6, Figure 12). These regions together formed the reaction zone which measured ~23 nm in depth from the surface of the sample. The entire reaction zone was characterized by a depletion in Ca, Fe, and Mg cations and an enrichment in Si (Figure 12). This agreed with RBS analysis for the sample

which are shown in Figure 7 where Ca, Fe, and Mg were all depleted as compared to the unaltered sample.

High fO2 (Magnetite-hematite buffer), 30 days

The high temperature sample (700ºC) VEN-7B (Figure 13) had an overall holohyaline texture with surficial, secondary phases randomly distributed across the surface (Figure 8). Some streaks of metal occurred rarely on the surface. TEM BF imaging showed a devitrification texture throughout the sample and along the surface (Figure 13). Alteration products were generally several microns in size and formed clumps of spots that measured ~10 μm in size (Figure 8). Composition of the secondary phase was not determined using SEM alone due to the small grain size however preliminary EDS analysis suggested this phase was an Fe oxide. TEM EDS analysis of the grain showed that it was Fe rich however quantitative measurements were not acquired for the grain because of unusually high thickness. Its composition can be inferred based on qualitative measurements (i.e. net counts) which was like those from section VEN-4B where the grains were confirmed to be magnetite. TEM EDS analysis revealed the lack of an alteration front however nano-scale phases rich in Ca, Fe, Mg, and Ti formed within the glass body and preferentially at the surface of the glass, likely because of devitrification. RBS analysis was not collected for this sample.

4.3 Alkaline basalts

Low fO2 (Graphite-carbon monoxide buffer), 14 days

The Venus surface temperature (470ºC) sample VEN-2 had an overall hypocrystalline texture that included mostly basaltic glass with microphenocrysts and microlites of olivine, clinopyroxene, plagioclase, and chromite that were still visible after experimentation (Figure 14). Streaks of metal occurred on the surface but were rare. The sampling area included a plagioclase

grain surrounded by a glassy matrix to measure the difference, if any, in alteration between glass and mineral. TEM BF imaging showed a glassy matrix with a honeycomb structure (Figure 15) and a plagioclase grain with a crystalline structure. TEM EDS analysis of the glassy region revealed a reaction zone that began at the surface and extended to a depth of ~39 nm characterized by an enrichment of Ca by ~1 wt% and Si by ~2 wt% (region B, Figure 16). TEM EDS analysis of the plagioclase grain confirmed the phase is labradorite ($(Ca_{0.6}Na_{0.4})(Si_{0.6}Al_{0.4})_4O_8$) and showed no zone of alteration (Figure 16). This agreed with RBS analysis for the sample which showed little to no indication of alteration (Figure 7).

The high temperature (700˚C) sample VEN-6 had an overall hypocrystalline texture and a rough surface. The surface roughness obfuscated many nano- to microscale phases that were present on the glass surface after experimentation, as shown in Figure 14. Streaks of metal occurred on the surface but were rare. TEM BF imaging showed a glassy matrix with a honeycomb structure however the honeycomb pattern was somewhat subdued because of the unusually high thickness of the sample (~120 nm). TEM EDS analysis showed a surface layer of crystalline material that extended from the surface of the sample to a depth of ~63 nm (region C, Figure 17) and was characterized by an enrichment in Ca by ~8 wt% and Fe by ~12 wt% (Table 6). Below region C is region B which extended to a depth of ~58 nm and was characterized by an enrichment in Al by ~ 4 wt%, Si by ~8 wt% and a depletion in Mg by ~1 wt% (Table 6, Figure 17). The entire reaction zone measured ~121 nm in depth and was characterized by an enrichment in Ca, Fe, and Si and a depletion in Mg. RBS analysis for this sample was not collected.

High fO2 (Magnetite-hematite buffer), 14 days

The Venus surface temperature (470ºC) sample VEN-5A had an overall hypocrystalline texture with a rough surface. The surface roughness obfuscated many nano- to microscale phases that were present on the glass surface after experimentation, as shown in Figure 14. Streaks of metal occurred on the surface but were rare. SEM imaging showed small grains (~1 μm) of an Fe rich mineral that occurred on the surface and one such grain was included in the sampling area for TEM analysis. TEM BF imaging showed a glassy matrix with a honeycomb structure and nanocrystalline material in the near surface. In addition to the nanocrystalline material near the surface, there were several Ca carbonate grains that measured ~200 nm in diameter and a crystalline Fe oxide grain that measured ~350 nm in diameter. TEM SAED analyses confirmed the Ca carbonate phase was calcite and the Fe oxide phase was magnetite. TEM EDS analysis of the glassy region showed the presence of a reaction zone that began at the surface of the sample and extended ~12 nm into the sample body (Figure 18). The reaction zone was characterized by a Ca enrichment by ~3 wt%, an Fe enrichment by ~2 wt%, an Al depletion by ~2 wt% and a K depletion by ~1 wt% (Table 4; region B, Figure 18). This agreed with RBS analysis for the sample which are shown in Figure 7 where Fe was enriched as compared to the unaltered sample.

The high temperature (700˚C) sample VEN-4A had an overall hypocrystalline texture with a rough surface. The surface roughness obfuscated many nano- to microscale phases that were present on the glass surface after experimentation, as shown in Figure 14. Streaks of metal occurred on the surface but were rare. SEM imaging showed small grains (~1 μm) of an Fe rich mineral phase that occurred on the surface. TEM BF imaging showed a glassy matrix with a honeycomb texture where pockets of nano- to microcrystalline material existed as well as

nanocrystalline phase(s) concentrated at the surface of the sample (Figure 19). The nanocrystalline material at the surface was Fe rich while the nano to microcrystalline material within the pockets that make up the honeycomb texture was rich in Ca, Fe, Mg, and Ti and was assumed to be the result of some amount of devitrification of the sample during experimentation. Quantitative analysis of the region that experienced devitrification was excluded from the description of the reaction zone. The thin, dark layer visible at the surface of the basalt glass in Figure 18 was enriched in Fe by ~23 wt% and is likely magnetite. The reaction zone began at the surface of the sample, extended to a depth of ~36 nm and was characterized by an enrichment of Ca by ~3 wt% and Fe by ~10 wt% and a depletion of Al by ~2 wt% and Si by ~6 wt% (region B, Figure 19). This agreed with the RBS analysis which showed an enrichment in Fe (Figure 7).

Section 5: Discussion

Experimental conditions, including basalt composition, oxygen fugacity (fO_2), temperature, and time, were all treated as independent variables in our investigation of basalt alteration (Table 3). The formation of secondary phases, such as Fe oxides, was predicted to occur under more oxidizing (near the M-H buffer) conditions and conversely expected not to occur under more reducing (near the G-CO buffer) conditions. Oxidation was predicted to occur via cation diffusion whereby basalt was oxidized by the removal of cations rather than the addition of oxygen species. Extent (or thickness) of alteration fronts were expected to increase with the square root of time, or with the increase in reaction temperature. Different starting compositions (tholeiitic versus alkaline basalt) were hypothesized to alter in different manners, including the formation or lack thereof of reaction products and/or different rates of reaction. To test these hypotheses, a series of experiments were conducted to isolate each independent variable. This experimental approach confirmed that outward cation diffusion is the dominant mechanism of chemical alteration of basalts, and that basalts on the surface of Venus could be as young as ~40 to ~241,000 years old.

5.1 Varying experimental temperature conditions

Tholeiitic basalts subjected to the same pressure conditions (90 bars) and oxygen fugacities (near the M-H buffer), but differing temperatures (470°C, 700°C), have varying reaction fronts over the same experimental duration (15 days, Figure 20). Basalt VEN-4B reacted under high temperature (700ºC) developed a reaction front that advanced ~23 nm while basalt VEN-5B reacted under surface temperature (470ºC) developed a reaction front that advanced ~16 nm. Both sample surfaces were coated with discontinuous iron oxide grains, confirmed to be

magnetite (Fe_3O_4) in VEN-4B, supporting the observation that cations are mobilized during reaction.

Alkaline basalts subjected to the same pressure conditions (90 bars) and oxygen fugacities (near the M-H buffer), but differing temperatures (470°C, 700°C), also have varying reaction front thicknesses over an experimental duration of 15 days (Figure 21). Basalt VEN-4A reacted under high temperature (700ºC) developed a reaction front that advanced ~36 nm while basalt VEN-5A reacted under surface temperature (470ºC) developed a reaction front that advanced ~ 12 nm. Both sample surfaces developed discontinuous coatings of magnetite.

The effect of temperature on the reaction zone was more pronounced for the alkaline basalt than the tholeiitic basalt. However, the high temperature alkaline basalt VEN-4A began to devitrify during experimentation, thereby complicating its use in comparing glass alteration (Figure 22). Regardless, temperature, and thus, diffusion of cations, clearly exerts a control on the formation of a reaction zone. Since high temperature (700°C) reaction conditions favored greater Fe oxide production and serve as a proxy for geologic time, these results confirm that cation diffusion is a dominant mechanism for basalt glass alteration.

5.2 Varying experimental oxygen fugacity conditions

Basalt samples of tholeiitic composition subjected to the same temperature (470°C) and pressure conditions (90 bars), but differing oxygen fugacities (more reducing, near the G-CO buffer, versus more oxidizing, near the M-H buffer) differed in either the presence or absence of a reaction zone over the same experimental run time (15 days, Figure 23). Basalt VEN-1, reacted in a less oxidizing atmosphere (near the G-CO buffer), developed grains of graphite on the surface and a reaction front penetrating into the sample was not observed. Basalt VEN-5B,

reacted in a more oxidizing atmosphere (near the M-H buffer), developed grains of Fe oxide on the surface and simultaneously developed a reaction front that advanced ~16 nm into the sample, confirming the hypothesis that cation diffusion occurs via oxidation processes. The absence or presence of a reaction front based on experimental oxygen fugacity conditions indicates that oxygen fugacity exerts a control on the formation of a reaction zone, and consequently, chemical alteration of basalt. Since Venus has a more oxidizing environment (fO_2 near the M-H buffer), the style and rate of chemical alteration observed in the basalts reacted in a highly oxidizing environment should be comparable.

5.3 Varying starting basalt compositions

Basalt samples subjected to the same temperature and pressure conditions (470ºC, 90 bars), oxygen fugacities (near the M-H buffer), alteration time (15 days), but varying in starting basalt composition (alkaline basalt versus tholeiitic basalt) have similar reaction fronts, but different overall glass structure and secondary phases (Figure 24). Tholeiitic basalt VEN-5B developed a reaction front that advanced ~16 nm while alkaline basalt VEN-5A developed a reaction front that advanced ~12 nm. Both basalt surfaces were coated with discontinuous Fe oxide grains and VEN-5A was coated with discontinuous calcite ($CaCO_3$) grains, suggesting that basalt glass alteration is dominated by cation diffusion. Furthermore, the production of a reaction front of similar thickness for samples of different starting composition supports the notion that cation diffusion is the dominant mechanism of alteration. The structure of the glass for alkaline basalt VEN-5A changed during reaction, forming a honeycomb pattern where pockets measuring ~10-20 nm in diameter enriched in Ca, Fe, Mg, and Ti cations were surrounded by Al-, Si-rich glass. This texture extended from the surface of the sample through the entire FIB section (~5 μm) and differed from tholeiitic basalt VEN-5B, which remained glassy after alteration. The

observed honeycomb texture was interpreted as the beginning of devitrification, where given more time and/or higher temperature, nanocrystals of olivine and/or pyroxene and/or spinel would begin to crystallize within the pockets. This observation was confirmed by high temperature (700ºC) alkaline basalt VEN-4A, where a similar honeycomb texture was observed and nanocrystalline material formed within the pockets. The glass transition in basalt has been estimated to occur from ~650ºC to ~725ºC based on studies of nepheline-normative and olivine tholeiitic basalts (Ryan and Sammis 1981; Cooper et al. 1996), and was therefore exceeded during high temperature experimentation for alkaline basalts. The most obvious effect of varying basalt composition is the glass morphology after experimentation, where alkaline basalt glass has a wavy, mottled surface texture that tholeiitic basalt glass does not have.

5.4 Varying experimental duration conditions

Tholeiitic basalts subjected to the same temperature and pressure conditions (700ºC, 90 bars), oxygen fugacities (near the M-H buffer), but differing durations of experimentation (15 days versus 30 days), have similar alteration products but different reaction fronts (Figure 25). Both samples developed discontinuous grains of Fe oxide on the surface because of oxidation, however the grains formed more cohesive clumps (measuring ~10 μm in diameter) over the 30-day experimental duration (VEN-7B) when compared to the 15-day duration (VEN-4B) where grains were several hundred nanometers to a couple of microns in size. The production of larger clumps of Fe oxide on the sample VEN-7B as compared to VEN-4B supports they hypothesis that alteration products will increase with increasing time. Along the surface of the sample and throughout the sample body, VEN-7B developed nanocrystals of augite, olivine, and spinel, indicative of devitrification. Cook et al. (1990) and Cooper et al. (1996) found that the thickness of a reaction front was related to the square root of time and we anticipated the same result.

However, because sample VEN-7B lacked a reaction front (likely obscured by devitrification), this hypothesis could not be tested here.

5.5 Rates of reaction

The reaction zones of samples who were subjected to experimental conditions for 15 days can be measured and used to calculate a rate of reaction. Sample VEN-5B experienced oxidizing conditions (i.e., near the M-H buffer) and a temperature of 470ºC for 15 days and developed a reaction front that advanced ~16 nm. Using the thickness of the weathering rind formed in 15 days at surface temperature and assuming a linear relationship between time and reaction front advancement, it would take ~26 years to generate a reaction front that would be thick enough (~10 μm) to detect using spectroscopic techniques. This implies that basalts on the surface of Venus could be as young as ~40 years old. This result supports that of Filiberto et al. (2020) which found that oxidation of olivine could produce a sufficiently thick coating of Fe oxide (enough to obscure any olivine spectra) within months to years.

Sample VEN-4B experienced oxidizing conditions (i.e., near the M-H buffer) and a temperature of 700ºC for 15 days and developed a reaction front that advanced ~23 nm. The higher temperature (700ºC) condition served as a proxy for geologic time, thus demonstrating that alteration increases with increasing time. The amount of Fe oxide that developed on the surface also increased with increasing temperature (i.e. time), as seen by comparing the surfaces of VEN-5B and VEN-4B (Figure 8).

While the relationship between time and reaction front advancement could not be tested here, it has been suggested by Cooper et al. (1996) that the reaction front advances non-linearly with the square root of time following an Arrhenius relation. Additionally, the style of alteration

described by Cook et al. (1990) and Cooper et al. (1996) was rate-limited by cation diffusion, which agrees with the findings in this study. Therefore, applying an Arrhenius analysis to our data yields values for activation energy of diffusion (E_a) and the diffusivity as temperature approaches infinity (D_0). These values can be used to determine the diffusivity of cations at any temperature (T) using the Arrhenius relation (equation 4):

$$D = D_0 e^{-Ea/RT} \qquad \text{eq. (4)}$$

where D is diffusivity (measured in m^2/s) and R is the gas constant. Figure 26 shows diffusivity plotted as a function of temperature from 426ºC to 1600ºC and generally shows how diffusivity increases with increasing temperature. The diffusivity values of cations within the reaction front, or weathering rind, are expressed in m^2/s and thus can be expressed as a one-dimension thickness (i.e. thickness of rind from surface of basalt to interior) by multiplying by time. Figure 27 shows how results from this study can be used to extrapolate alteration rind thickness over geologic timescales, assuming continuous diffusion. Assuming the threshold of detection of a weathering rind from thermal emissivity data collected from an orbiter would require several microns (5 – 10 μm) of altered material, our data suggests that a basalt on the surface could be as young as 268 to 1068 years for a glassy tholeiitic basalt and 475 to 1,900 years for a glassy alkaline basalt.

Section 6: Summary

Several studies have suggested that volcanic activity on the surface of Venus is more recent than previously thought, potentially as recent as several hundreds of thousands of years ago to presently active (Smrekar et al. 2010; Stofan et al. 2016; D'Incecco et al. 2017; Filiberto et al. 2020). These studies have relied on interpretations of thermal emissivity data and chemical weathering experiments, however few experiments have focused on weathering within non-terrestrial (i.e. without H_2O) atmospheres. This study utilized an experimental approach to characterize the products and mechanisms of basalt alteration for the surface of Venus under non-terrestrial (i.e. CO_2-rich) atmospheric conditions. Our basalts developed nano- to microscale alteration, on their surfaces and at depth, that were characterized and quantified using microscopic techniques including scanning electron microscopy (SEM) and transmission electron microscopy (TEM) energy dispersive X-ray (EDS) analysis. Results presented here suggest that basalts on Venus undergo reaction at the surface via outward cation diffusion because of the oxidation potential created by the CO_2-rich atmosphere, and the rate of alteration can be constrained by our results (Cook et al. 1990; Cooper et al. 1996; Zolotov 2018). While our experiments could not confirm the non-linear relationship between extent of alteration (i.e. thickness of alteration front) and time proposed by Cooper et al. (1996) and others, we are able to establish a lower limit on the rate of alteration for basalts on the surface of Venus assuming the reactions proceed as observed where cation diffusion is the rate-limiting step in alteration.

Alteration of basalt glass was driven by cation diffusion where cations diffused from depth to the free surface, consistent with previous studies of basalt (Cook et al. 1990; Cooper et al. 1997; Berger et al. 2019). Altered basalts were characterized by a reaction front that began at the surface and extended several nanometers (ranging from ~16nm to ~121nm) into the basalt.

The reaction front was characterized by an enrichment of divalent cations Ca^{2+}, Fe^{T}, and Mg^{2+} at or near the surface and a depletion of these cations but enrichment of Al and Si at a greater depth. Additionally, alteration of basalt glass resulted in the formation of micro-scale grains of the Fe oxide phase magnetite (Fe_3O_4). While the Fe oxide phase hematite (Fe_2O_3) was not observed on any of our basalts, it is predicted to occur on the surface of basalts on Venus (Zolotov et al. 2018). The lack of observed hematite could be due an insufficient experimental duration required to convert magnetite to hematite, a process recently observed when oxidizing olivine (Filiberto et al. 2020).

The rate-limiting factor of basalt alteration is the diffusion of network-modifying cations to the free surface, observed by the increased concentration of Ca^{2+}, Mg^{2+}, and Fe^{T} cations as well as Fe oxides on the surface. The extent of reaction, or the thickness of the reacted zone, was therefore controlled by the rate of cation diffusion. While we were not able to compare the effect of experimental duration on alteration, we can still calculate rates of reaction for samples reacted for 15 days assuming cation diffusion is the rate-limiting step in alteration and that extent of alteration is proportional to the square root of time. Because several microns of material are required to determine composition via spectral analyses, we can assume that a 5 to 10 μm thick layer of alteration would be discernable in thermal emissivity spectra (Smrekar et al. 2010). Therefore, basalts on the surface could be as young as 268 to 1,900 years. If interpretations of varying emissivity by Smrekar et al. (2010) are correct, basalts observed by the VIRTIS spectrometer in 2006 could be anywhere from 282 years to 1,914 years old.

Section 7: Future Work

This study is part of a larger project whose goal is to characterize basalt-atmosphere interaction on the surface of Venus using rocks and atmospheres like those observed on Venus. Future work will investigate the effect of SO_2 and CO_2 on basalt alteration, where SO_2 is expected to interact with the surface to produce secondary minerals not expected or observed under the presence of CO_2 alone. Future work will include longer experimental durations (e.g. 30 days) to determine the relationship between extent of alteration and time.

While the approach used in this study to understand the interaction between basalt glass and Venus atmosphere confirmed potential reaction mechanisms and products, the applicability of our results could be improved. Extrapolating our rates of reaction to age date basalts on Venus is complicated by the fact that none of our basalt glasses formed continuous surfaces of Fe oxide(s), which are assumed to be the cause of the observed thermal emissivity anomalies (Smrekar et al. 2010). While a ~10 μm thick reaction front may form in the timespan of 268 – 1,900 years, its current detectability may rely on the thickness of Fe oxide(s) phases alone. Future work needs to be done to understand the necessary time frame required to form continuous coatings of Fe oxide on basalt glasses. Additionally, spectral libraries for weathered basalts, and specifically basaltic glass, need to be collected in appropriate atmospheres for the most accurate application of our results. While basalts on the surface of Venus are expected to be glassy, building spectral libraries for major mineral phases of would be useful for interpretations of old data and for informing new missions. Future missions that aim to reach the surface with a lander or rover vehicle could consider taking *in-situ* geochemical analyses from the surface and below in step-wise fashion as to uncover potential geochemical layers and thus, time records of basalts.

List of references

Barsukov, V. L., V. P. Volkov, and I. L. Khodakovsky. 1982. “The Crust of Venus: Theoretical Models of Chemical and Mineral Composition.” Journal of Geophysical Research 87 (Supplement): A3–9. https://doi.org/10.1029/jb087is01p000a3.

Bender, J.F., F.N. Hodges, and A.E. Bence. 1978. “Petrogenesis of Basalts from the Project FAMOUS Area: Experimental Study from 0 to 15 Kbars.” Earth and Planetary Science Letters 41 (3): 277–302. https://doi.org/10.1016/0012-821X(78)90184-X.

Berger, Gilles, Annick Cathala, Sébastien Fabre, Anastassia Y. Borisova, Alain Pages, Thierry Aigouy, Jerôme Esvan, and Patrick Pinet. 2019. “Experimental Exploration of Volcanic Rocks-Atmosphere Interaction under Venus Surface Conditions.” Icarus, March. https://doi.org/10.1016/J.ICARUS.2019.03.033.

Cooper, Reid F., John B. Fanselow, and David B. Poker. 1996. “The Mechanism of Oxidation of a Basaltic Glass: Chemical Diffusion of Network-Modifying Cations.” Geochimica et Cosmochimica Acta 60 (17): 3253–65. https://doi.org/10.1016/0016-7037(96)00160-3.

D’Incecco, Piero, Nils Müller, Jörn Helbert, and Mario D’Amore. 2017. “Idunn Mons on Venus: Location and Extent of Recently Active Lava Flows.” *Planetary and Space Science* 136 (December 2016): 25–33. https://doi.org/10.1016/j.pss.2016.12.002.

Fegley, B., G. Klingelhöfer, R.A. Brackett, N. Izenberg, D.T. Kremser, and K. Lodders. 1995a. “Basalt Oxidation and the Formation of Hematite on the Surface of Venus.” Icarus 118 (2): 373–83. https://doi.org/10.1006/ICAR.1995.1197.

Fegley, Bruce, and Allan H Treiman. 1992. “Chemistry Of Atmosphere-Surface Interactions On Venus And Mars.” https://doi.org/10.1029/GM066p0007.

Fegley, Bruce, Mikhail Yu. Zolotov, and Katharina Lodders. 1997. “The Oxidation State of the Lower Atmosphere and Surface of Venus.” Icarus 125 (2): 416–39. https://doi.org/10.1006/ICAR.1996.5628.

Filiberto, Justin. 2014. “Magmatic Diversity on Venus: Constraints from Terrestrial Analog Crystallization Experiments.” Icarus 231 (March): 131–36. https://doi.org/10.1016/J.ICARUS.2013.12.003.

Filiberto, Justin, David Trang, Allan H. Treiman, and Martha S. Gilmore. 2020. “Present-Day Volcanism on Venus as Evidenced from Weathering Rates of Olivine.” Science Advances 6 (1): eaax7445. https://doi.org/10.1126/sciadv.aax7445.

Gilmore, Martha, Allan Treiman, Jörn Helbert, and Suzanne Smrekar. 2017. “Venus Surface Composition Constrained by Observation and Experiment.” *Space Science Reviews* 212 (3–4): 1511–40. https://doi.org/10.1007/s11214-017-0370-8.

Head, James W., L. S. Crumpler, Jayne C. Aubele, John E. Guest, and R. Stephen Saunders. 1992. “Venus Volcanism: Classification of Volcanic Features and Structures, Associations, and Global Distribution from Magellan Data.” Journal of Geophysical Research 97 (E8): 13153. https://doi.org/10.1029/92JE01273.

Lewis, John S, and Frank A Kreimendahl. 1980. “Oxidation State of the Atmosphere and Crust of Venus from Pioneer Venus Results.” Icarus 42 (3): 330–37. https://doi.org/10.1016/0019-1035(80)90098-6.

Nimmo, F., and D. McKenzie. 1998. “VOLCANISM AND TECTONICS ON VENUS.” Annual Review of Earth and Planetary Sciences 26 (1): 23–51. https://doi.org/10.1146/annurev.earth.26.1.23.

Pieters, C. M., J. W. Head, W. Patterson, S. Pratt, J. Garvin, V. L. Barsukov, A. T. Basilevsky, et al. 1986. “The Color of the Surface of Venus.” Science 234 (4782): 1379–83. https://doi.org/10.1126/science.234.4782.1379.

Price, J. 2004. “The Cold Seal Apparatus.” Experimental Geochemistry Facilities. Assembled under E. Bruce Watson. http://ees2.geo.rpi.edu/exgeochemp/index.html

Ryan, Michael P., and Charles G. Sammis. 1981. “The Glass Transition in Basalt.” Journal of Geophysical Research: Solid Earth 86 (B10): 9519–35. https://doi.org/10.1029/JB086iB10p09519.

Skjelkvale, Brit-L, H E F Amundsen, Suzanne Y O’reilly, W L Griffin, and T Gjelsvik. 1989. “A PRIMITIVE ALKALI BASALTIC STRATOVOLCANO AND ASSOCIATED ERUPTIVE CENTRES, NORTHWESTERN SPITSBERGEN" VOLCANOLOGY AND TECTONIC SIGNIFICANCE.” Journal of Volcanology and Geothermal Research. Vol. 37.

Smrekar, Suzanne E, Ellen R Stofan, Nils Mueller, Allan Treiman, Linda Elkins-Tanton, Joern Helbert, Giuseppe Piccioni, and Pierre Drossart. 2010. “Recent Hotspot Volcanism on Venus from VIRTIS Emissivity Data.” Science (New York, N.Y.) 328 (5978): 605–8. https://doi.org/10.1126/science.1186785.

Stofan, Ellen R., Suzanne E. Smrekar, Nils Mueller, and Joern Helbert. 2016. “Themis Regio, Venus: Evidence for Recent (?) Volcanism from VIRTIS Data.” *Icarus* 271: 375–86. https://doi.org/10.1016/j.icarus.2016.01.034.

Treiman, Allan H. 2007. “Geochemistry of Venus’ Surface: Current Limitations as Future Opportunities.” In Geophysical Monograph Series, 176:7–16. American Geophysical Union (AGU). https://doi.org/10.1029/176GM03.

Treiman, H, and S P Schwenzer. 2009. “BASALT-ATMOSPHERE INTERACTION ON VENUS: PRELIMINARY RESULTS ON WEATHERING OF MINERALS AND BULK ROCK. A.” In LPSC XL.

Appendices

Appendix A: Figures and tables

Table 1. Concentrations of gasses that make up the Venusian atmosphere and their respective altitude within the atmosphere (Zolotov 2018).

Gas	Concentration	Altitude
CO_2	96.5 ± 0.8%	<65 km
N_2	3.5 ± 0.8%	<65 km
SO_2	150 ± 30 ppmv	22-42 km
H_2O	30 ± 15 ppmv	5-45 km
CO	17 ± 1.4 ppmv	12 km
COS	4.4 ± 1 ppmv	33 km
H_2S	3 ± 2 ppmv	<20km

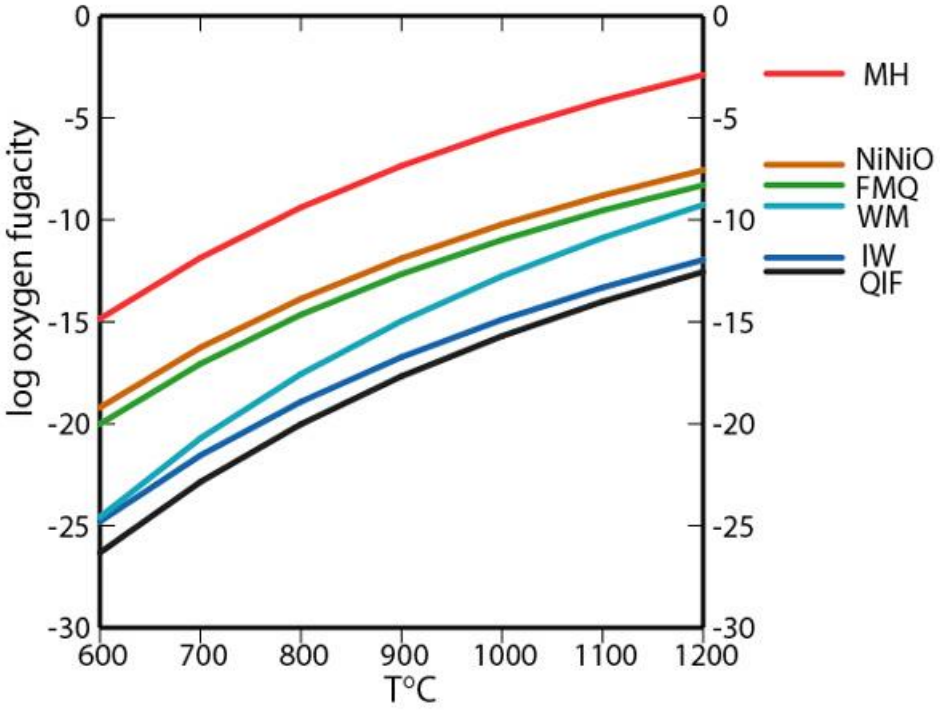

Figure 1. Log oxygen fugacity (or fO_2) versus temperature for several common mineral buffer assemblages at 1 bar pressure. The oxidation state at the surface of Venus is approximated to be near the magnetite-hematite (MH) buffer curve. Curves plotted from Frost (1991) and diagram from https://en.wikipedia.org/wiki/Mineral_redox_buffer.

Figure 2. Color image of the surface of Venus at the Venera 13 site, after white light illumination correction, from Pieters et al. (1987).

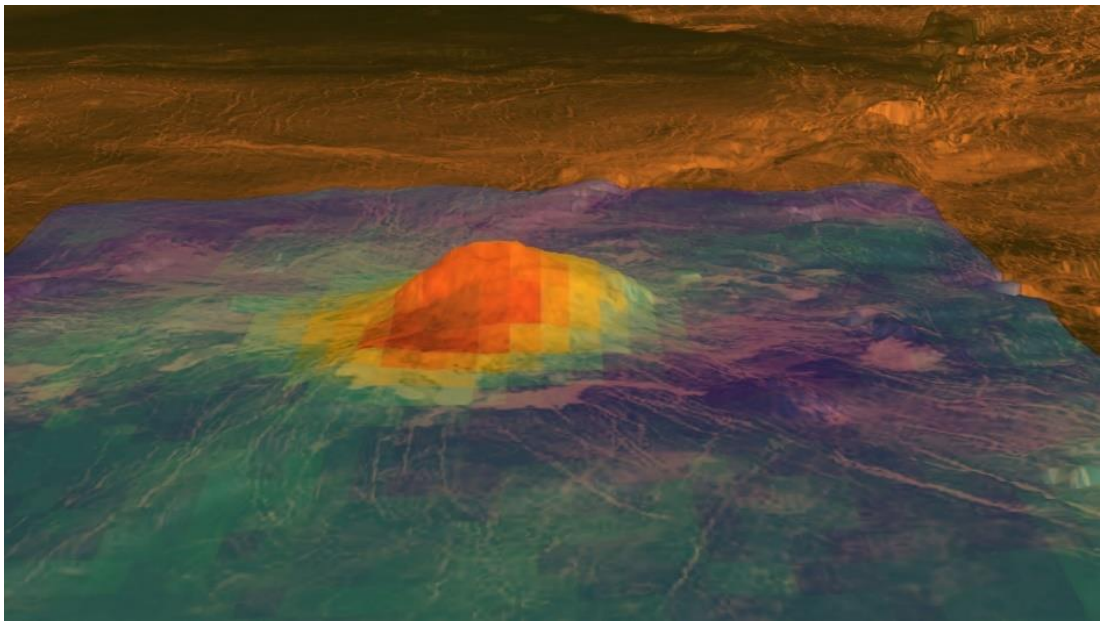

Figure 3. Thermal emissivity data for Idunn Mons showing the thermal anomaly centered around the volcano compared to the surrounding basaltic plains, from Smrekar (2010).

Table 2. Elemental bulk chemistry from *in-situ* XRF analyses (in wt. %, with 2 sigma errors) for three lander missions, from Filiberto (2014).

	Venera 13	**Venera 14**	**VEGA 2**
SiO_2	45.1 ± 6.0	48.7 ± 7.2	45.6 ± 6.4
TiO_2	1.6 ± 0.9	1.25 ± 0.8	0.2 ± 0.2
Al_2O_3	15.8 ± 6.0	17.9 ± 5.2	16.0 ± 3.6
FeO	9.3 ± 4.4	8.8 ± 3.6	7.7 ± 2.2
MnO	0.2 ± 0.2	0.16 ± 0.16	0.14 ± 0.24
MgO	11.4 ± 12.4	8.1 ± 6.6	11.5 ± 7.4
CaO	7.1 ± 2.0	10.2 ± 2.4	7.5 ± 1.4
K_2O	4.0 ± 1.2	0.2 ± 0.14	0.1 ± 0.16
SO_3	1.6 ± 2.0	0.35 ± 0.6	1.9 ± 1.2

Table 3. Experimental conditions for all samples, including sample ID, type of basaltic starting material, experimental temperature and pressure conditions, experimental duration, and experimental oxygen fugacity. Aside from run time, all possible experimental arrangements (varying temperature and oxygen fugacity conditions) were explored on both starting compositions.

sample name	chemical type	run conditions	run time	fO_2 conditions
VEN-1	tholeiite	470 C, 92 bars	15 days	G-CO buffer
VEN-2	alkaline	470 C, 92 bars	15 days	G-CO buffer
VEN-3	tholeiite	700 C, 90 bars	15 days	G-CO buffer
VEN-4A	alkaline	700 C, 90 bars	15 days	M-H buffer
VEN-4B	tholeiite	700 C, 90 bars	15 days	M-H buffer
VEN-5A	alkaline	470 C, 90 bars	15 days	M-H buffer
VEN-5B	tholeiite	470 C, 90 bars	15 days	M-H buffer
VEN-6	alkaline	700 C, 90 bars	15 days	G-CO buffer
VEN-7B	tholeiite	700 C, 90 bars	30 days	M-H buffer

Table 4. Compositions of starting materials in weight percent oxide, determined using EPMA analyses.

Wt. % oxides	Synthetic tholeiitic basalt	Natural alkaline basalt
SiO_2	48.9	47.9
TiO_2	1.3	2.8
Al_2O_3	18.2	18.0
Cr_2O_3	0.05	0.0
FeO	10.1	9.6
MnO	0.2	0.1
MgO	8.3	3.3
CaO	10.2	7.7
Na_2O	2.1	6.0
K_2O	0.2	2.7

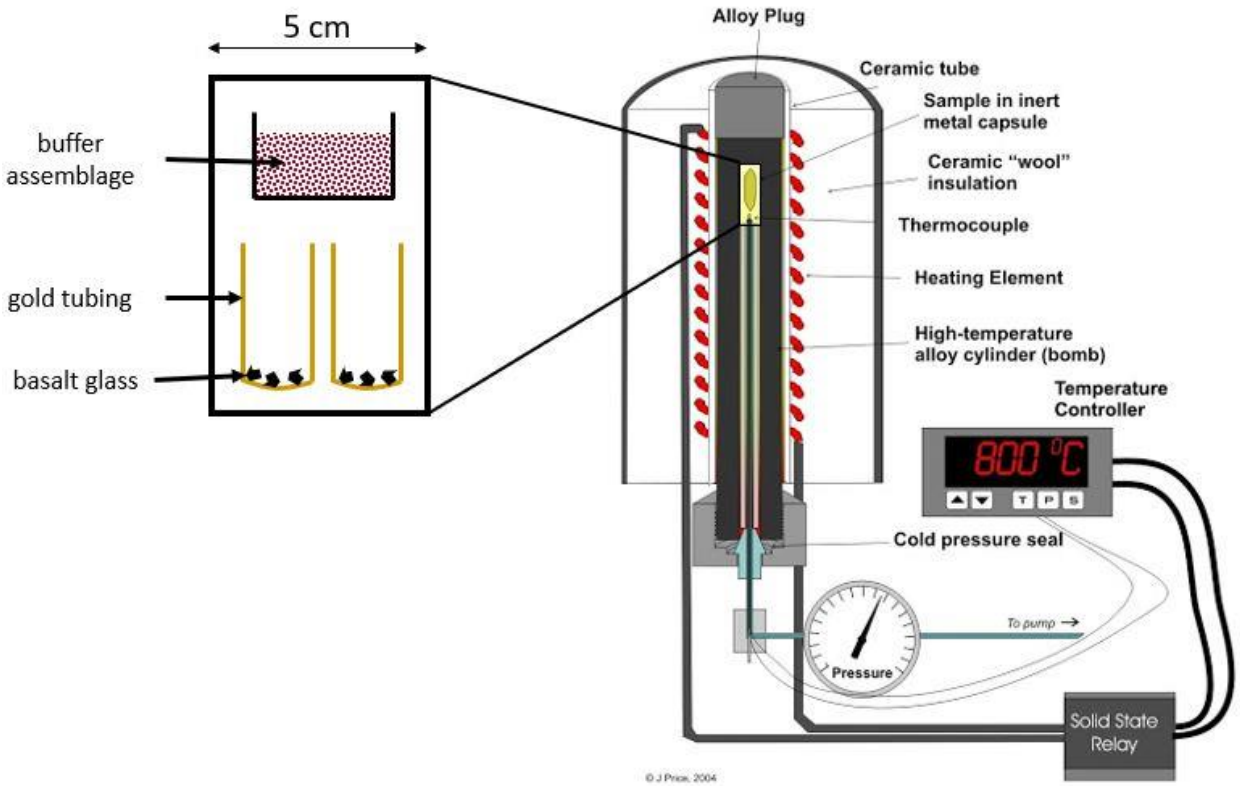

Figure 4. Schematic diagram depicting a standard cold-seal pressure vessel apparatus, highlighting the size and geometry of the sample chamber; figure modified from Price 2004.

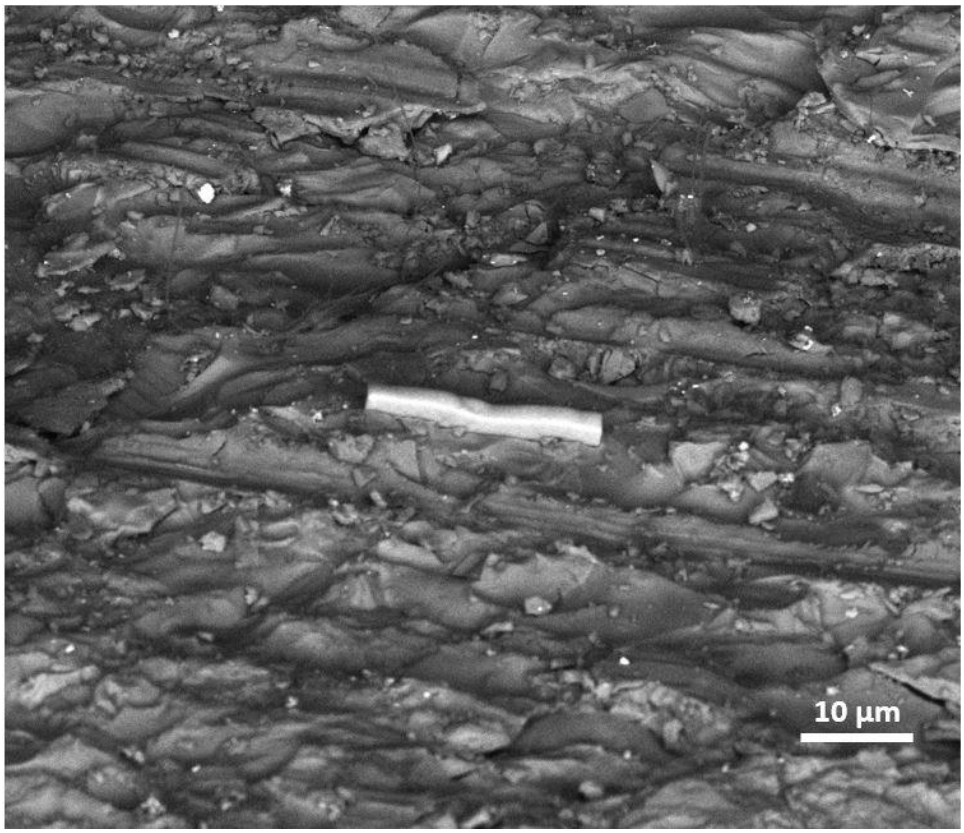

Figure 5. Backscatter electron image of sample VEN-4A with a carbon “cap” placed over the area of the sample that will be extracted and sectioned in preparation for TEM analysis.

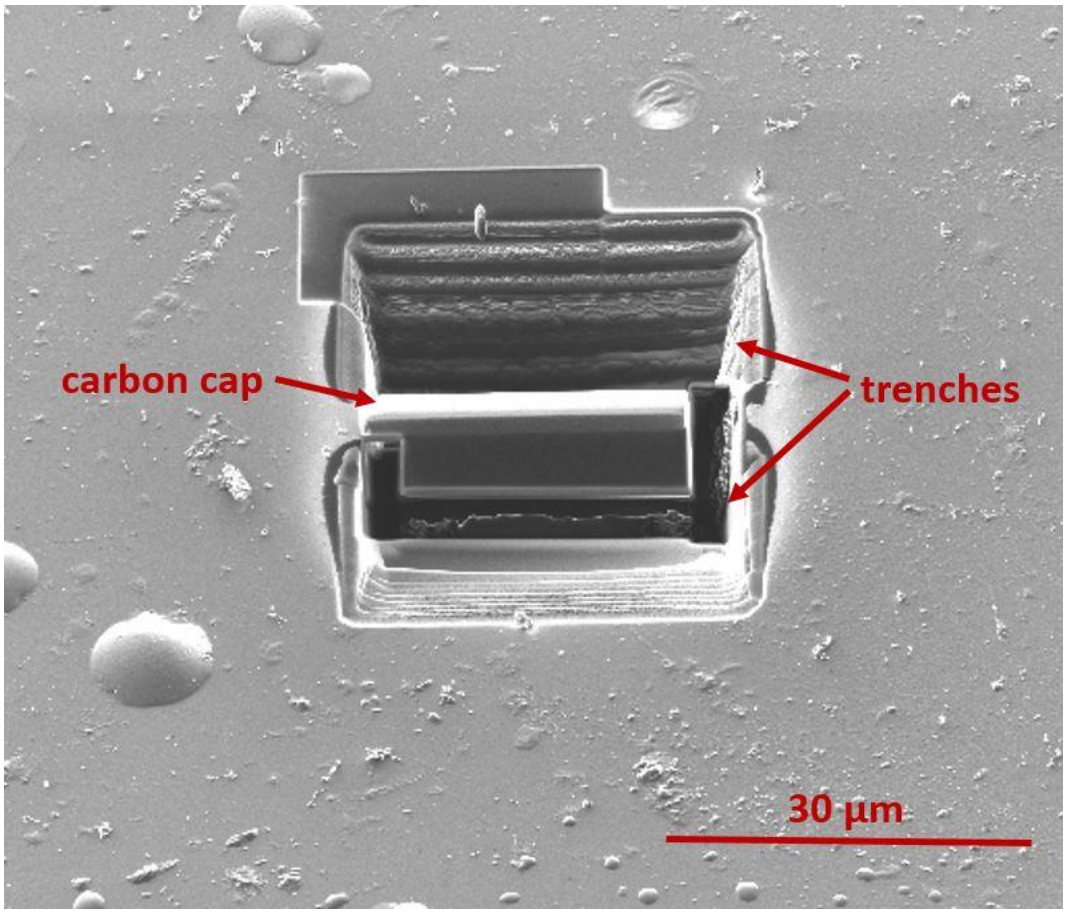

Figure 6. Backscatter electron image of sample VEN-1 with carbon cap placed over the area to be extracted as well as trenches which result from sample material being milled away.

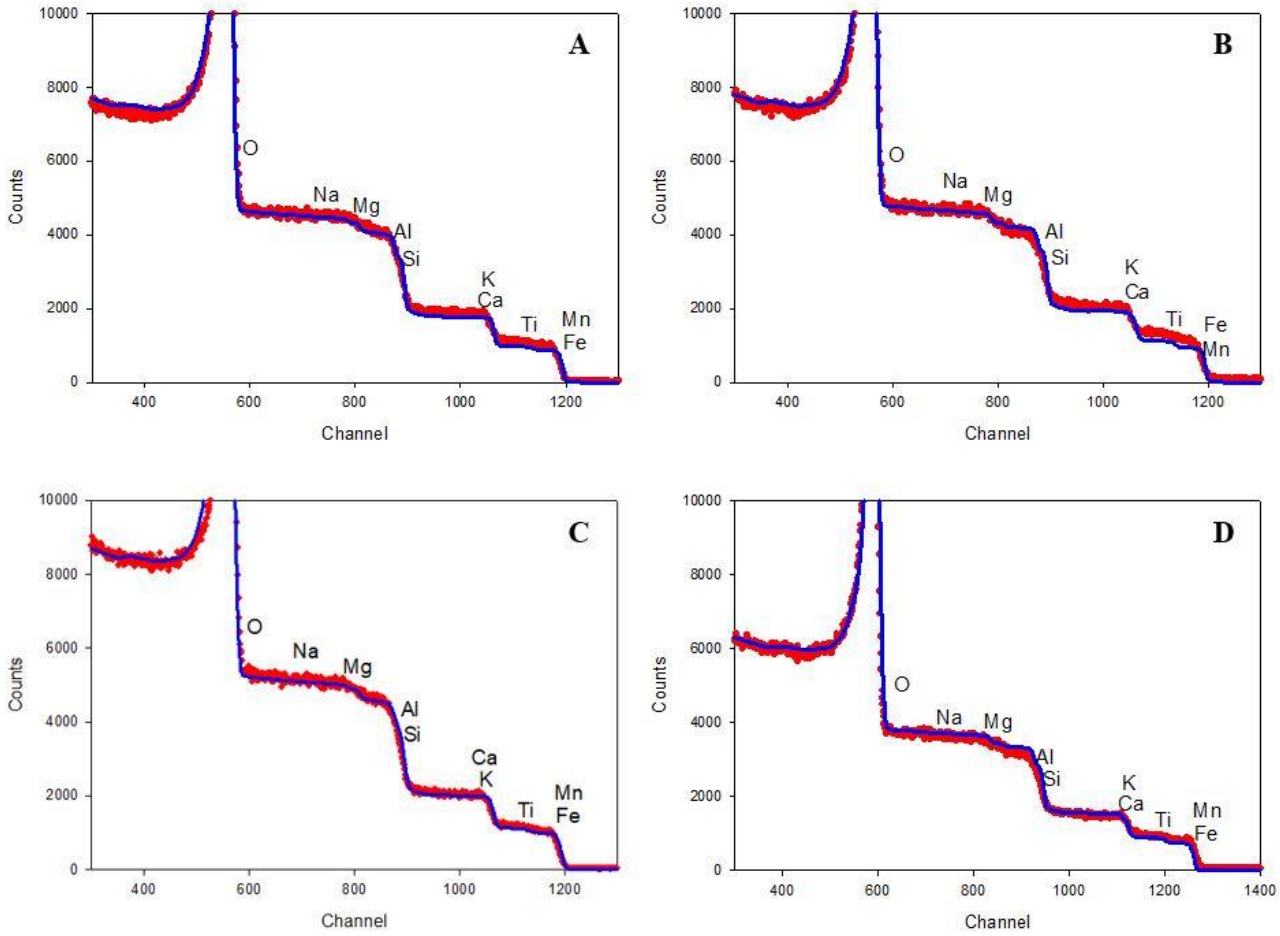

Figure 7. Spectra collected from weathered surfaces using Rutherford Backscattering Spectrometry (RBS) for samples (A) VEN-1 , (B) VEN-2, (C) VEN-3, (D) VEN-4A, (E) VEN-4B, (F) VEN-5A, and (G) VEN-5B. Simulated spectra for basalt glass (tholeiitic and alkaline) are shown by the blue line and the red points are the spectra collected from samples after experimentation. Spectra record composition from sample surface through ~1 μm depth into sample body.

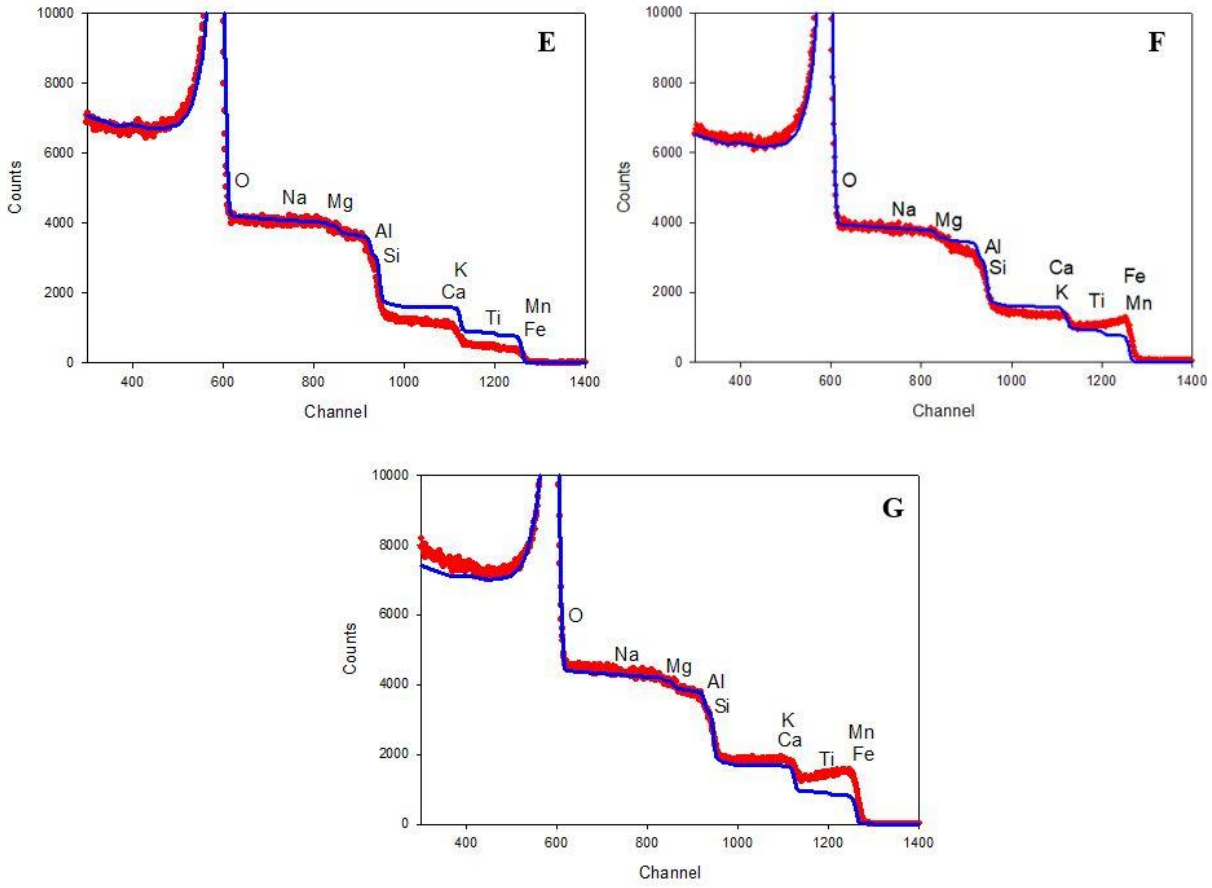

Figure 7. Cont.

Table 5. Compositions of unreacted basalt glasses prior to experimentation and reacted basalt glasses after experimentation in weight percent (wt %). Unreacted glass compositions determined by EPMA and recalculated from weight percent oxide; reacted glass compositions determined using TEM analyses. Weight percent analyses for reacted samples represent the average composition of the entire TEM section.

	unreacted tholeiite	unreacted alkaline	VEN-1		VEN-2		VEN-3		VEN-4A	
Si	22.8998	22.3857	27.0664	±0.6255	21.5311	±0.4674	27.5613	±0.5292	19.8192	±0.3280
Al	9.6324	9.5322	11.4750	±0.5676	9.6150	±0.4351	11.8214	±0.5214	8.5597	±0.3252
Fe	7.8742	7.42677	3.5497	±0.4967	8.9529	±0.7775	3.0828	±0.4066	12.4356	±0.6310
Mg	4.9811	2.0197	2.3373	±0.2767	1.8461	±0.2327	1.3338	±0.1879	2.3952	±0.2821
Ca	7.3042	5.4941	5.8917	±0.4788	5.1774	±0.3991	6.4127	±0.3968	9.4370	±0.3886
Na	1.5727	4.4678	0.9564	±0.2301	4.4569	±0.2757	0.6875	±0.1928	1.8697	±0.1886
K	0.1328	2.2647	0.2382	±0.1314	2.5800	±0.2426	0.1956	±0.1038	0.2313	±0.0856

	VEN-4B		VEN-5A		VEN-5B		VEN-6		VEN-7B	
Si	40.7424	±1.7973	27.2803	±0.4643	21.8889	±0.5056	25.8756	±0.3831	20.3269	±0.4274
Al	14.2314	±1.0647	7.8039	±0.3708	9.6022	±0.4672	10.5734	±0.4039	9.4048	±0.3899
Fe	6.6520	±1.2173	6.4598	±0.6167	8.0795	±0.8178	10.8158	±0.6301	5.8711	±0.5601
Mg	1.5045	±0.5251	1.5362	±0.1919	4.3787	±0.4311	1.1022	±0.1766	4.4041	±0.3287
Ca	10.6948	±1.1165	4.5483	±0.3671	8.5071	±0.5326	9.0657	±0.4016	9.6154	±0.4566
Na	1.0115	±0.3334	3.4803	±0.2048	1.7338	±0.2753	8.1150	±0.2876	1.0624	±0.1912
K	0.2741	±0.2194	1.1286	±0.1453	0.2543	±0.1323	0.3397	±0.1063	0.1564	±0.0740

.

Table 6. Cations by weight percent (with measured uncertainty) in the total reaction zones and geochemical regions (if any) of reacted basalt glasses compared to their average concentrations in the unreacted bulk sample.

	VEN-2		
	unreacted alkaline	reaction zone	
Si	22.3857	23.5764	±0.5010
Al	9.5322	10.1000	±0.6060
Fe	7.42677	9.0930	±0.8335
Mg	2.0197	1.8466	±0.2402
Ca	5.4941	5.5652	±0.4068
Na	4.4678	1.4042	±0.2075
K	2.2647	0.7424	±0.1619

	VEN-3						
	unreacted tholeiite	reaction zone		region B		region C	
Si	22.8998	27.3644	±0.6098	29.1915	±0.6153	24.6238	±0.6015
Al	9.6324	10.5896	±0.6117	10.4238	±0.6079	10.8382	±0.6174
Fe	7.8742	3.2842	±0.4159	2.7436	±0.3869	4.0950	±0.4595
Mg	4.9811	0.2551	±0.1197	0.4253	±0.1995	0	±0
Ca	7.3042	6.3258	±0.4333	5.6452	±0.3930	7.3466	±0.4938
Na	1.5727	4.1274	±0.4496	2.6266	±0.4006	6.3786	±0.5231
K	0.1328	0.3466	±0.1406	0.2609	±0.1308	0.4752	±0.1553

Table 6. (Continued)

	VEN-4A		
	unreacted alkaline	reaction zone	
Si	22.3857	16.3021	±0.2830
Al	9.5322	7.1618	±0.2667
Fe	7.42677	17.7121	±0.7118
Mg	2.0197	2.6643	±0.2831
Ca	5.4941	8.6730	±0.3741
Na	4.4678	2.5800	±0.2006
K	2.2647	0.1954	±0.0818

	VEN-4B						
	unreacted tholeiite	reaction zone		region B		region C	
Si	22.8998	42.1985	±2.2570	52.7750	±2.3065	21.0455	±2.1581
Al	9.6324	8.7154	±1.1637	9.5824	±1.1512	6.9813	±1.1887
Fe	7.8742	5.0291	±1.6027	3.2040	±1.2517	8.6792	±2.3046
Mg	4.9811	0.7134	±0.7094	0.6605	±0.4597	0.8192	±1.2088
Ca	7.3042	6.4851	±1.2510	3.3366	±0.7698	12.7820	±2.2134
Na	1.5727	7.3543	±0.9915	1.7907	±0.3398	18.4816	±2.2947
K	0.1328	0.1088	±0.1088	0.1632	±0.1632	0.0000	±0.0000

Table 6. (Continued)

	VEN-5A		
	unreacted alkaline	reaction zone	
Si	22.3857	21.5959	±0.4846
Al	9.5322	6.7412	±0.3605
Fe	7.42677	9.5726	±0.8099
Mg	2.0197	2.2368	±0.3115
Ca	5.4941	8.3156	±0.4191
Na	4.4678	5.9341	±0.3166
K	2.2647	1.2652	±0.1776

	VEN-5B						
	unreacted tholeiite	reaction zone		region B		region C	
Si	22.8998	21.7168	±0.6811	27.6149	±0.6173	15.8188	±0.7449
Al	9.6324	8.4658	±0.5991	9.2009	±0.5299	7.7308	±0.6683
Fe	7.8742	8.3910	±1.0846	6.6425	±0.7315	10.1395	±1.4376
Mg	4.9811	4.0800	±0.5534	2.6577	±0.3162	5.5023	±0.7907
Ca	7.3042	8.6170	±0.6271	5.0425	±0.4343	12.1915	±0.8199
Na	1.5727	2.9204	±0.5186	0.6282	±0.2192	5.2126	±0.8179
K	0.1328	0.5545	±0.2123	0.1818	±0.1206	12.1915	±0.3040

Table 6. (Continued)

	VEN-6						
	unreacted alkaline	reaction zone		region B		region C	
Si	22.3857	24.0710	±0.3789	30.1096	±0.4125	18.3391	±0.3479
Al	9.5322	9.2607	±0.3842	13.4677	±0.4621	5.2769	±0.3106
Fe	7.42677	13.1936	±0.7074	6.7024	±0.5186	19.3631	±0.8874
Mg	2.0197	1.2019	±0.1926	1.0133	±0.1870	1.3886	±0.1989
Ca	5.4941	9.6883	±0.4217	5.8795	±0.3022	13.2556	±0.5324
Na	4.4678	10.6666	±0.3680	5.5714	±0.2119	15.5429	±0.5187
K	2.2647	0.3655	±0.1150	0.2449	±0.0952	0.4766	±0.1341

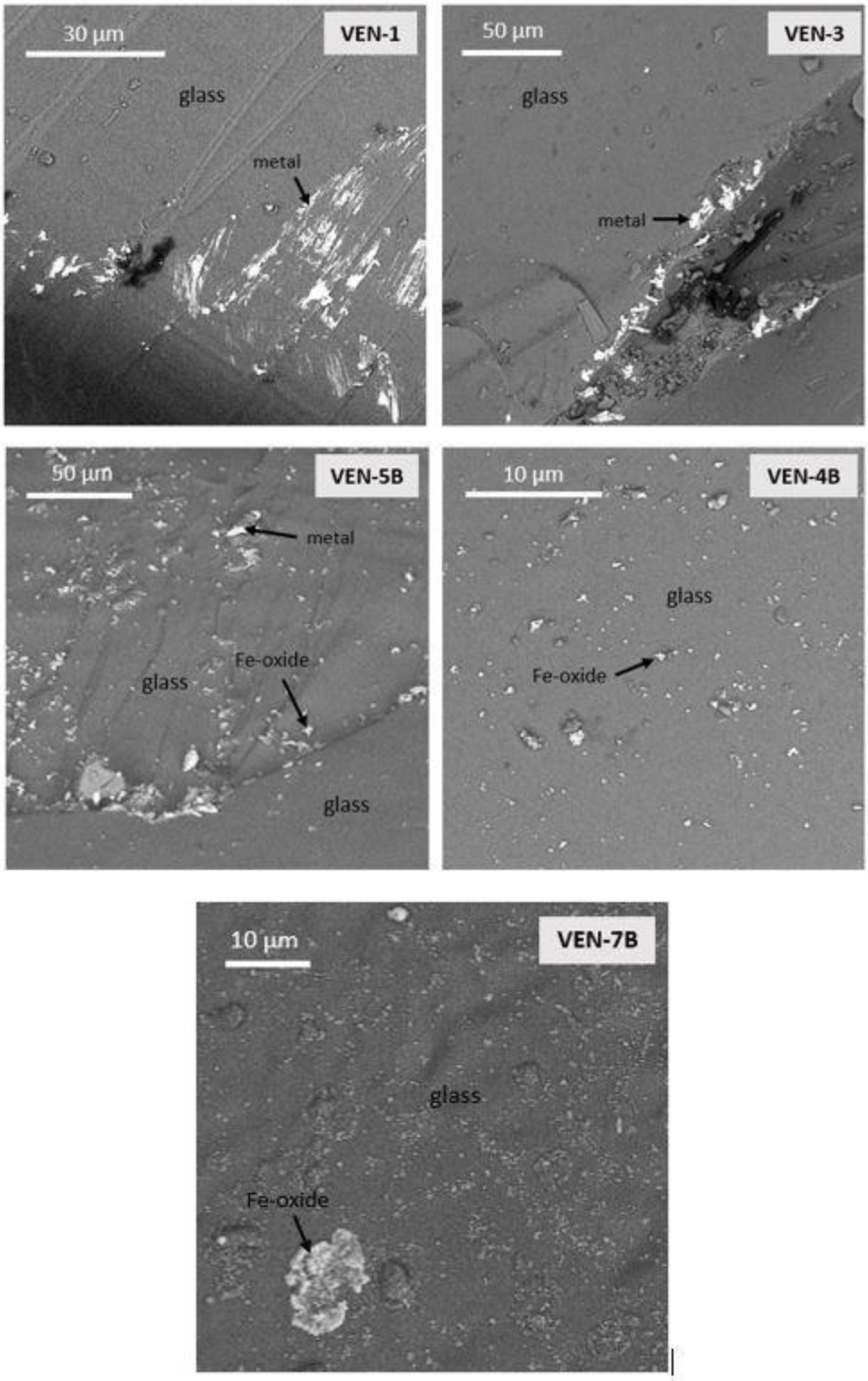

Figure 8. SEM backscatter electron (BSE) images for tholeiitic basalt samples after experimentation at varying oxygen fugacities (fO_2) and temperatures over a span of 14 days. Experimental conditions for each sample are found in Table 1.

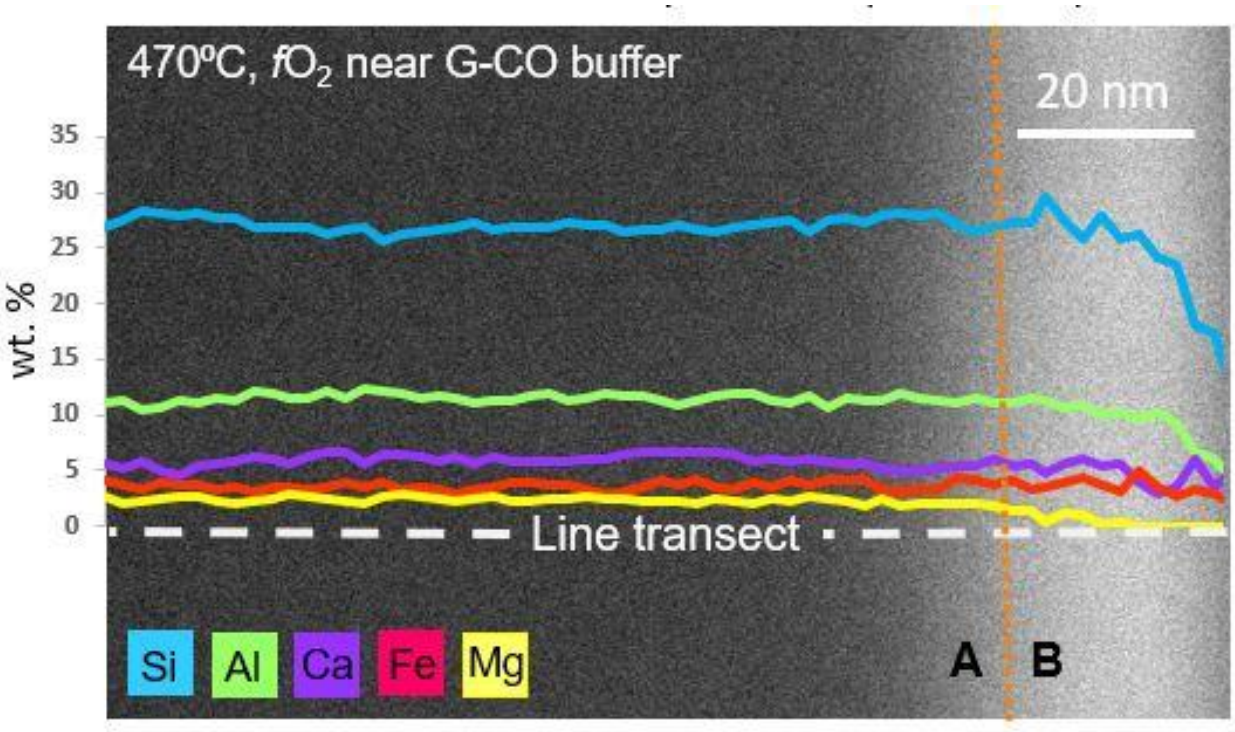

Figure 9. Line transect through sample VEN-1 with chemical analyses in weight percent (wt%). Region A is unaltered basalt glass, and region B is the carbon cap applied to protect the surface of the sample (e.g. the atmosphere during experimentation).

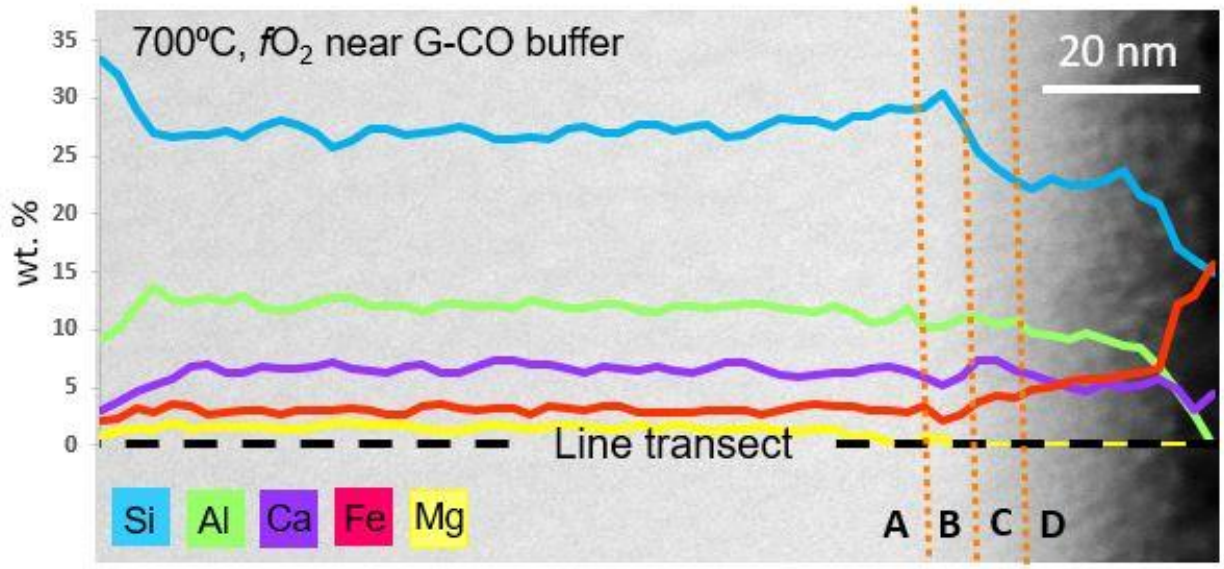

Figure 10. Line transect through sample VEN-3 with chemical analyses in weight percent (wt%). Region A is unaltered basalt glass, region B is the "depleted" region, region C is the "enriched" regions, and region D is the carbon cap applied to protect the surface of the sample (e.g. the atmosphere during experimentation).

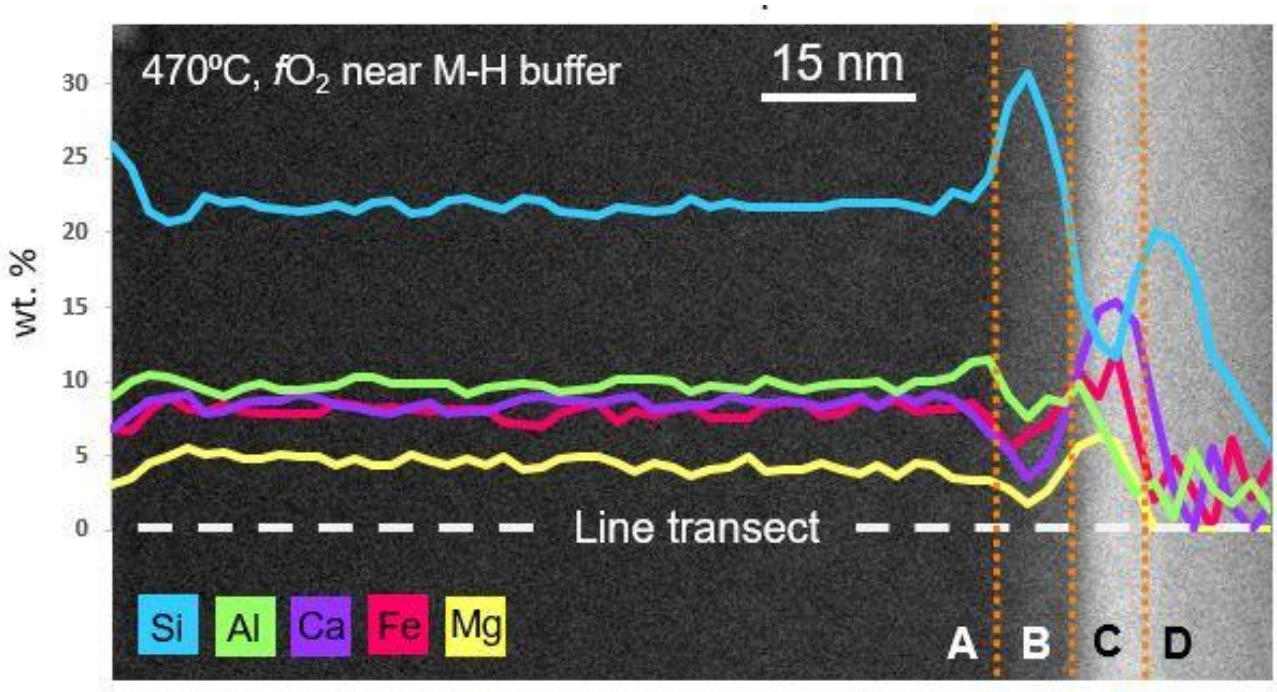

Figure 11. Line transect through sample VEN-5B with chemical analyses in weight percent (wt%). Region A is unaltered basalt glass, region B is the "depleted" region, region C is the "enriched" region (also the sample surface), and region D is the carbon cap applied to protect the surface of the sample (e.g. the atmosphere during experimentation).

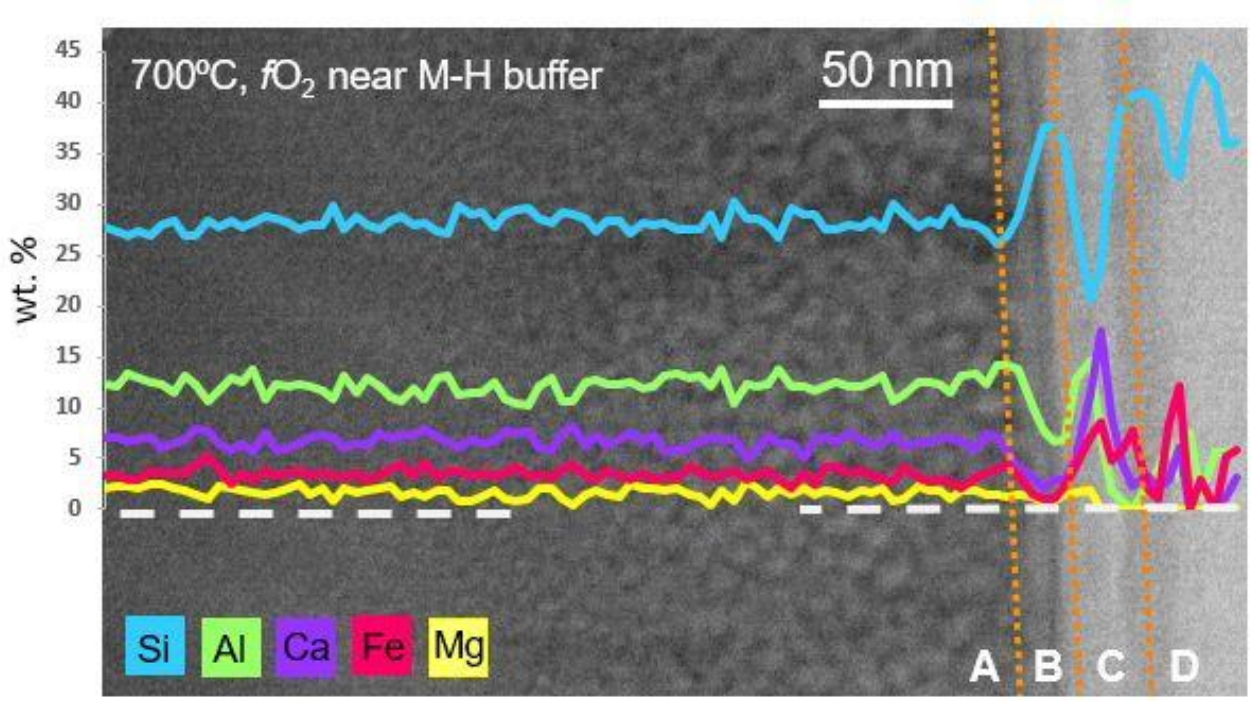

Figure 12. Line transect through sample VEN-4B with chemical analyses in weight percent (wt%). Region A is unaltered basalt glass, region B is the "depleted" region, region C is the "enriched" region (also the sample surface), and region D is the carbon cap applied to protect the surface of the sample (e.g. from the atmosphere during experimentation).

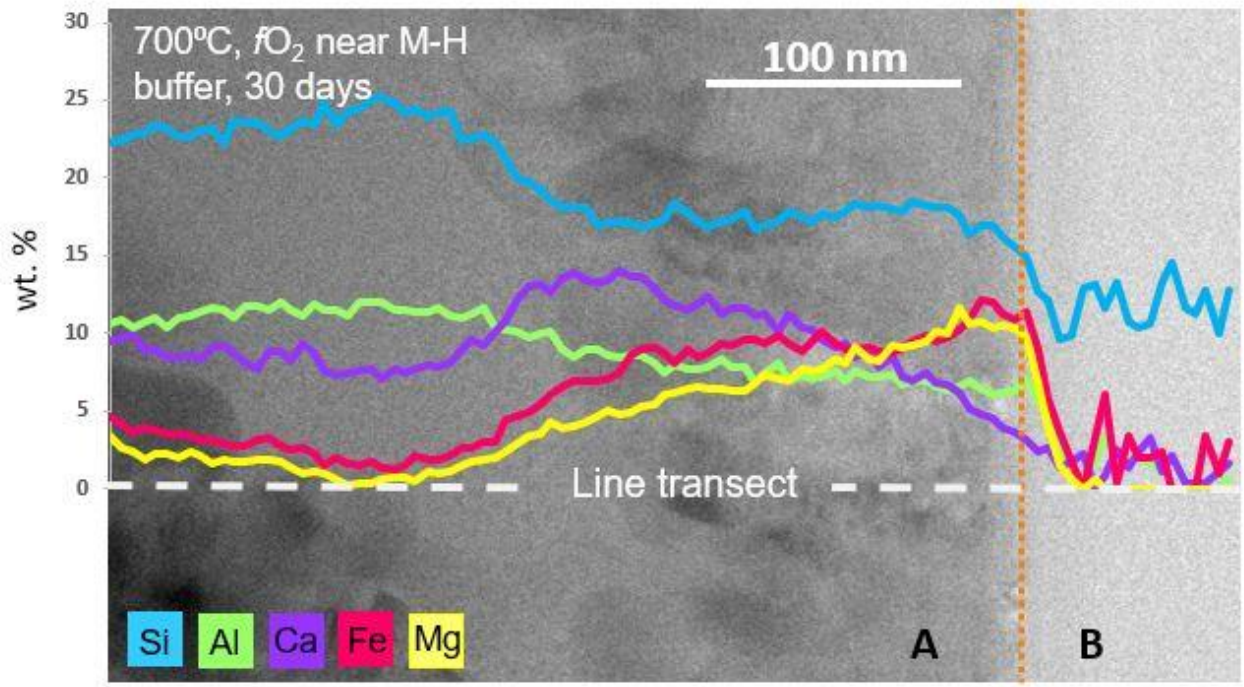

Figure 13. Line transect through sample VEN-7B with chemical analyses in weight percent (wt%). Region A is unaltered basalt glass and region B is the carbon cap applied to the surface of the sample (e.g. the atmosphere during experimentation).

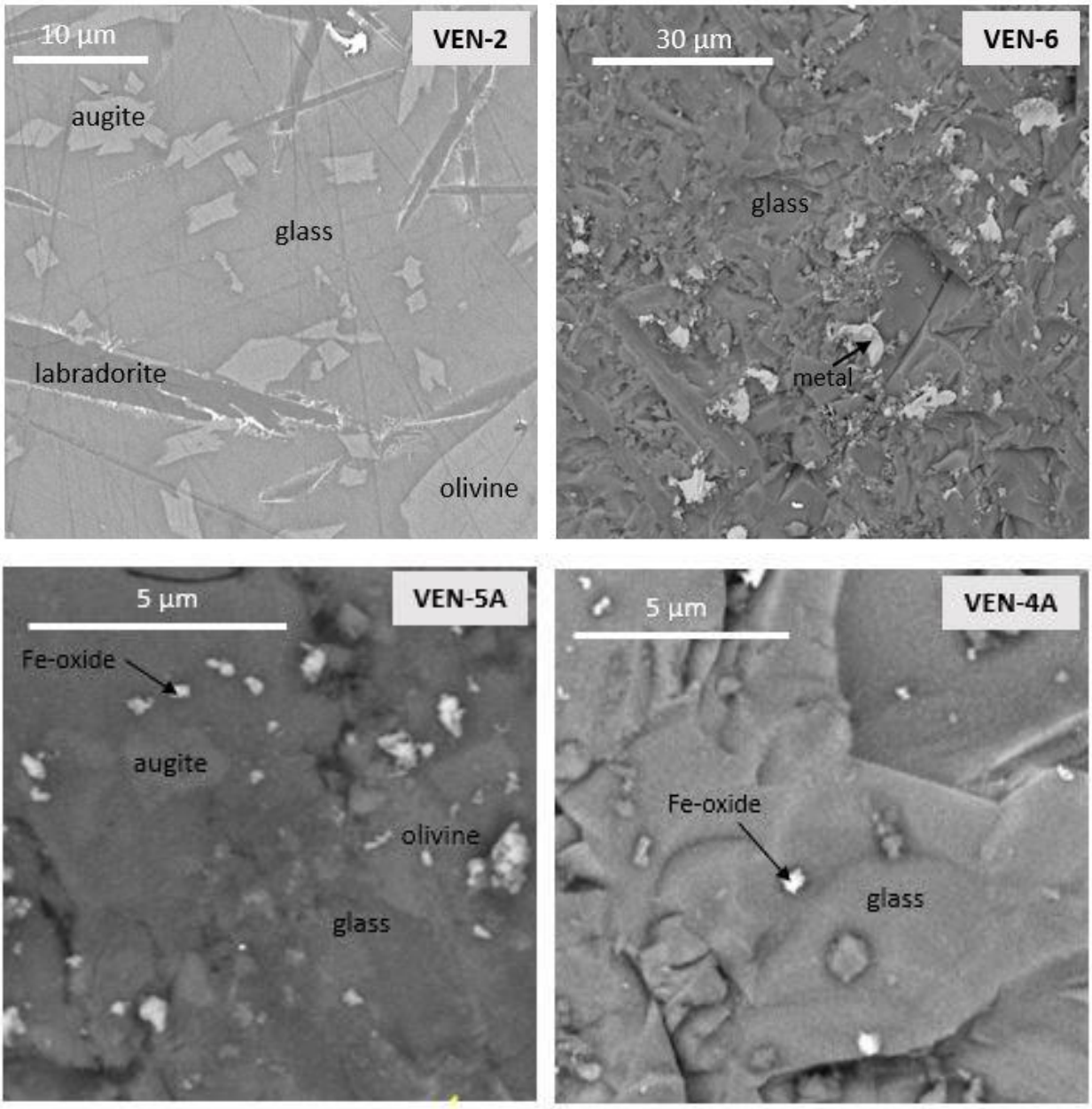

Figure 14. SEM backscatter electron (BSE) images for alkaline basalt samples after experimentation at varying oxygen fugacities (fO_2) and temperatures over a span of 14 days. Experimental conditions for each sample are found in Table 1.

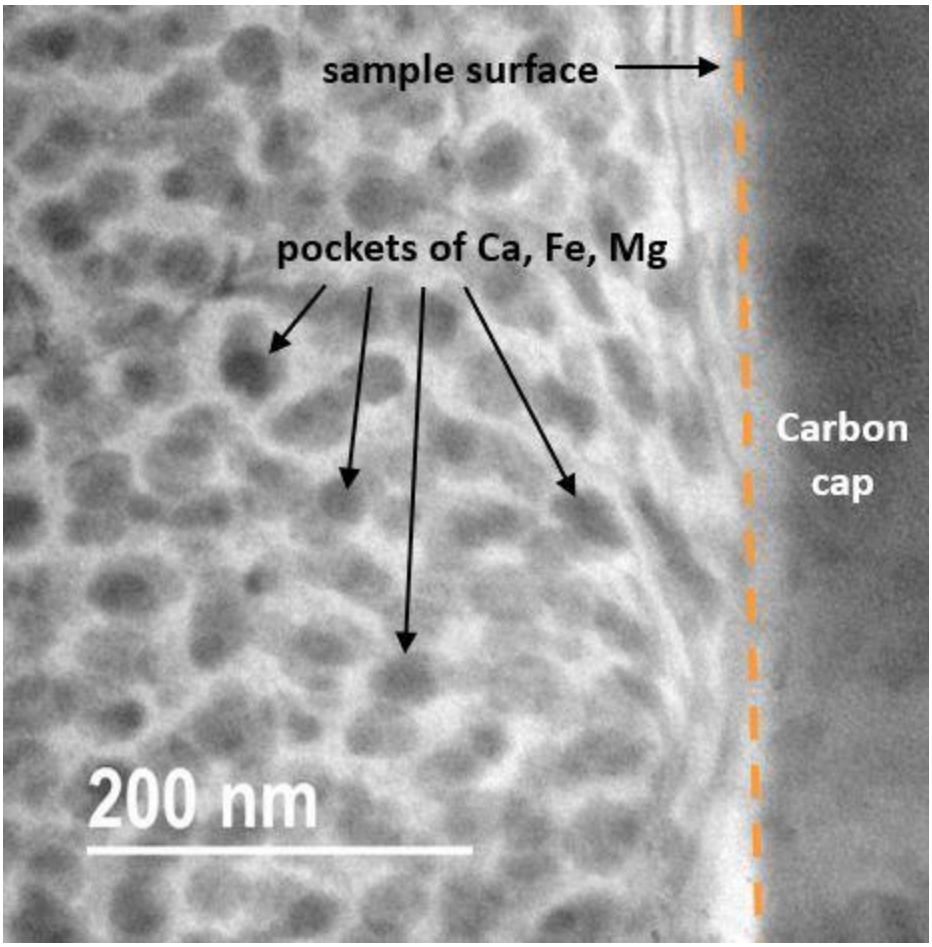

Figure 15. BSE TEM image of VEN-5A showing an example of the honeycomb texture observed in samples VEN-2, VEN-4A, VEN-5A, and VEN-6. Darker spots within the glass body are characterized by higher amounts of Ca, Fe, and Mg as compared to the surrounding, lighter colored interstitial feldspathic glass.

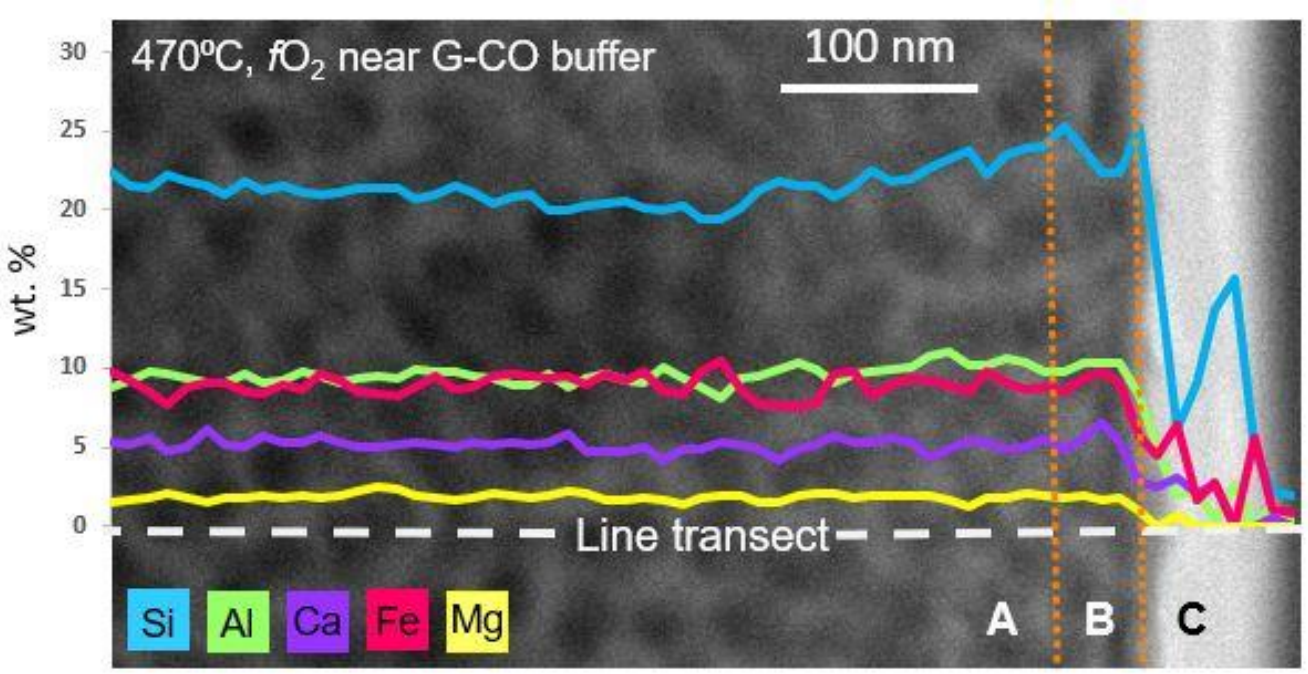

Figure 16. Line transect through sample VEN-2 with chemical analyses in weight percent (wt%). Region A is unaltered basalt glass, region B is the reaction zone, and region C is the carbon cap applied to the surface of the sample (e.g. the atmosphere during experimentation).

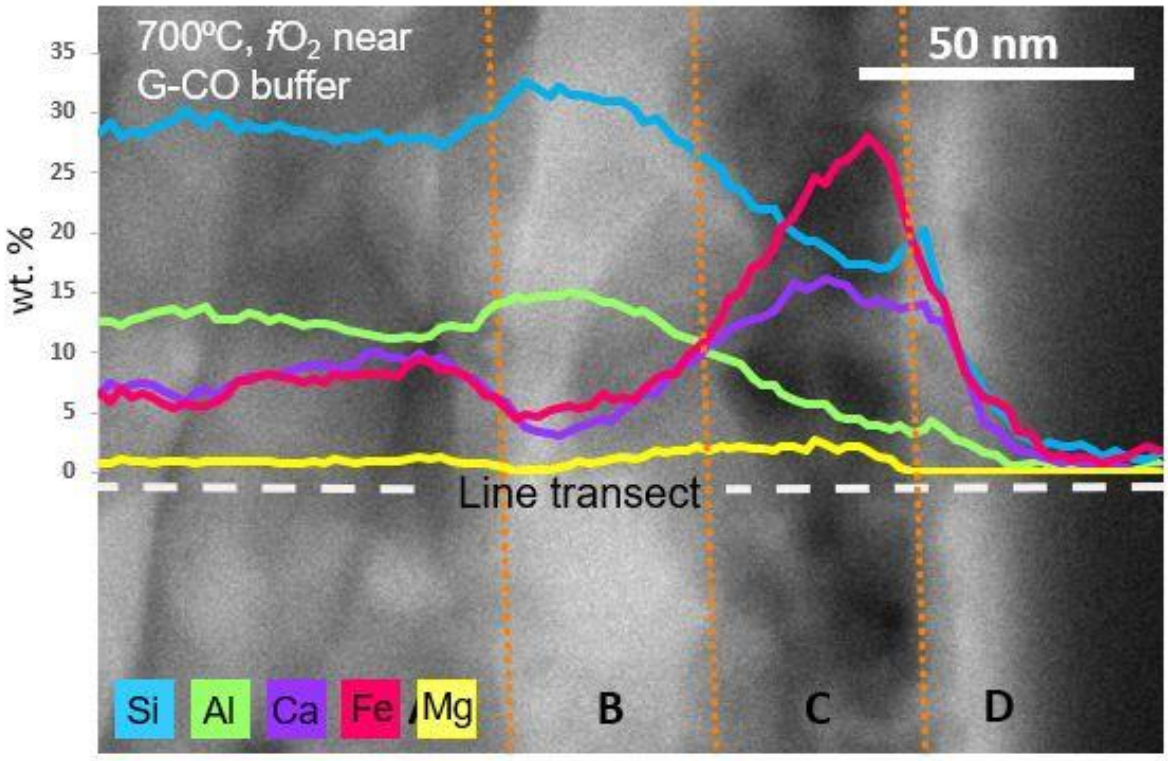

Figure 17. Line transect through sample VEN-6 with chemical analyses in weight percent (%). Region A is the unaltered basalt glass, region B is the feldspathic glassy region, region C is the crystalline region, and region D is the carbon cap applied to the surface of the sample (e.g. the atmosphere during experimentation).

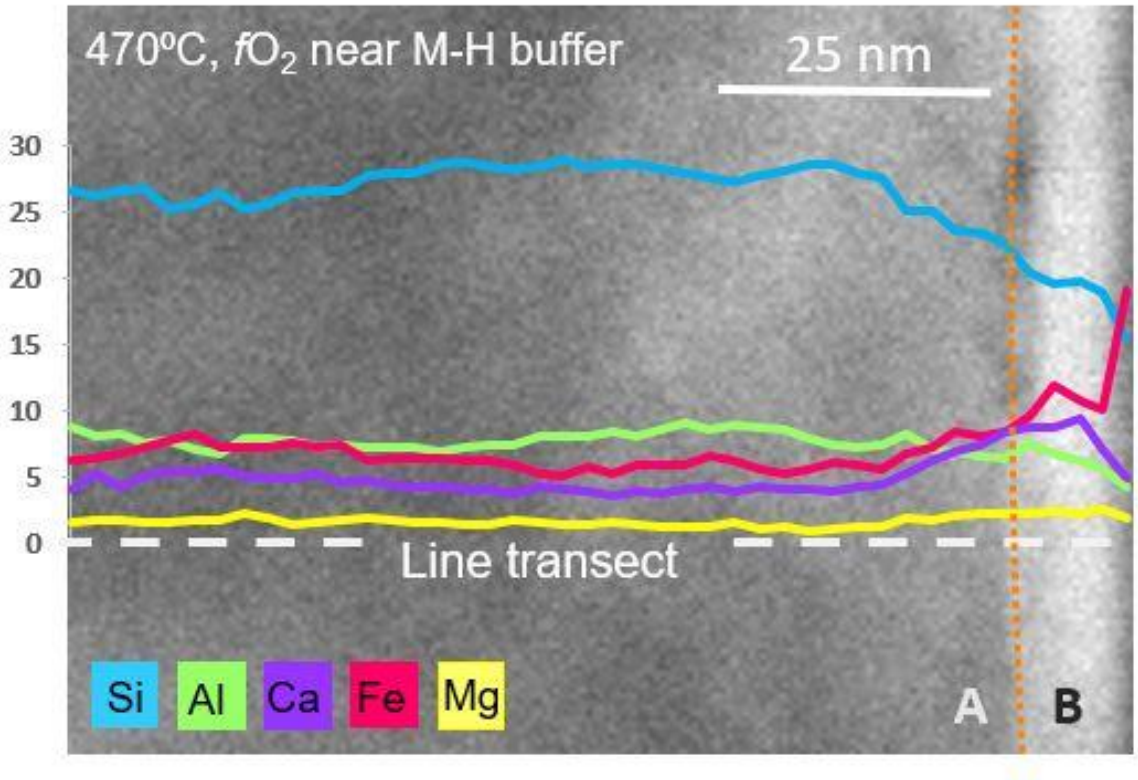

Figure 18. Line transect through sample VEN-5A with chemical analyses in weight percent (wt%). Region A is the alkaline basalt glass body and region B is the carbon cap applied to the surface of the sample (e.g. the atmosphere during experimentation).

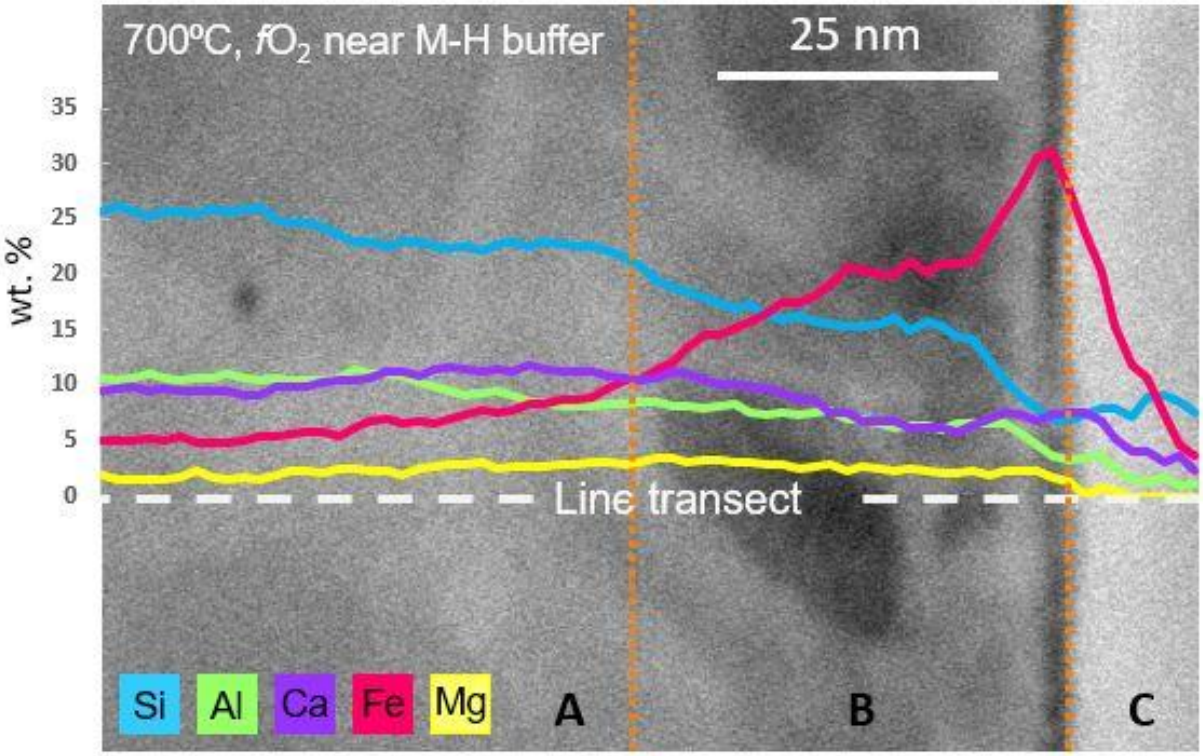

Figure 19. Line transect through sample VEN-4A with chemical analyses in weight percent (wt%). Region A is the alkaline basalt glass body and region B is the carbon cap applied to the surface of the sample (e.g. the atmosphere during experimentation).

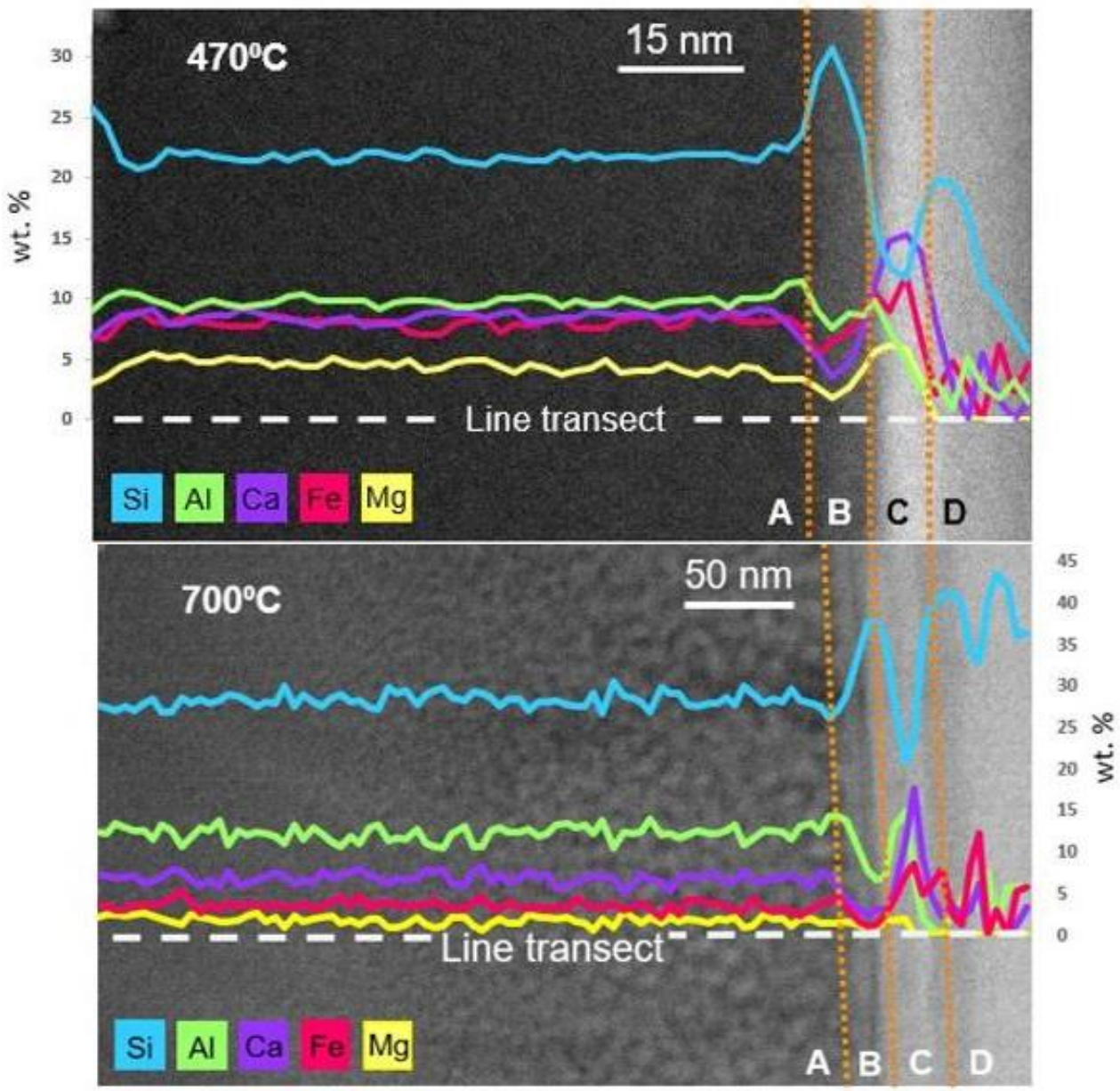

Figure 20. Side-by-side comparison of samples with the same initial starting composition (tholeiitic basalt) subjected to the same oxygen fugacity, pressure, and time conditions but differing temperature conditions. Sample on the top (VEN-5B) was subjected to surface temperatures (470ºC) and sample on the bottom (VEN-4B) was subjected to a higher temperature than that expected at the surface in order to account for some amount of geologic time (700ºC). Note the different scales on the vertical axes.

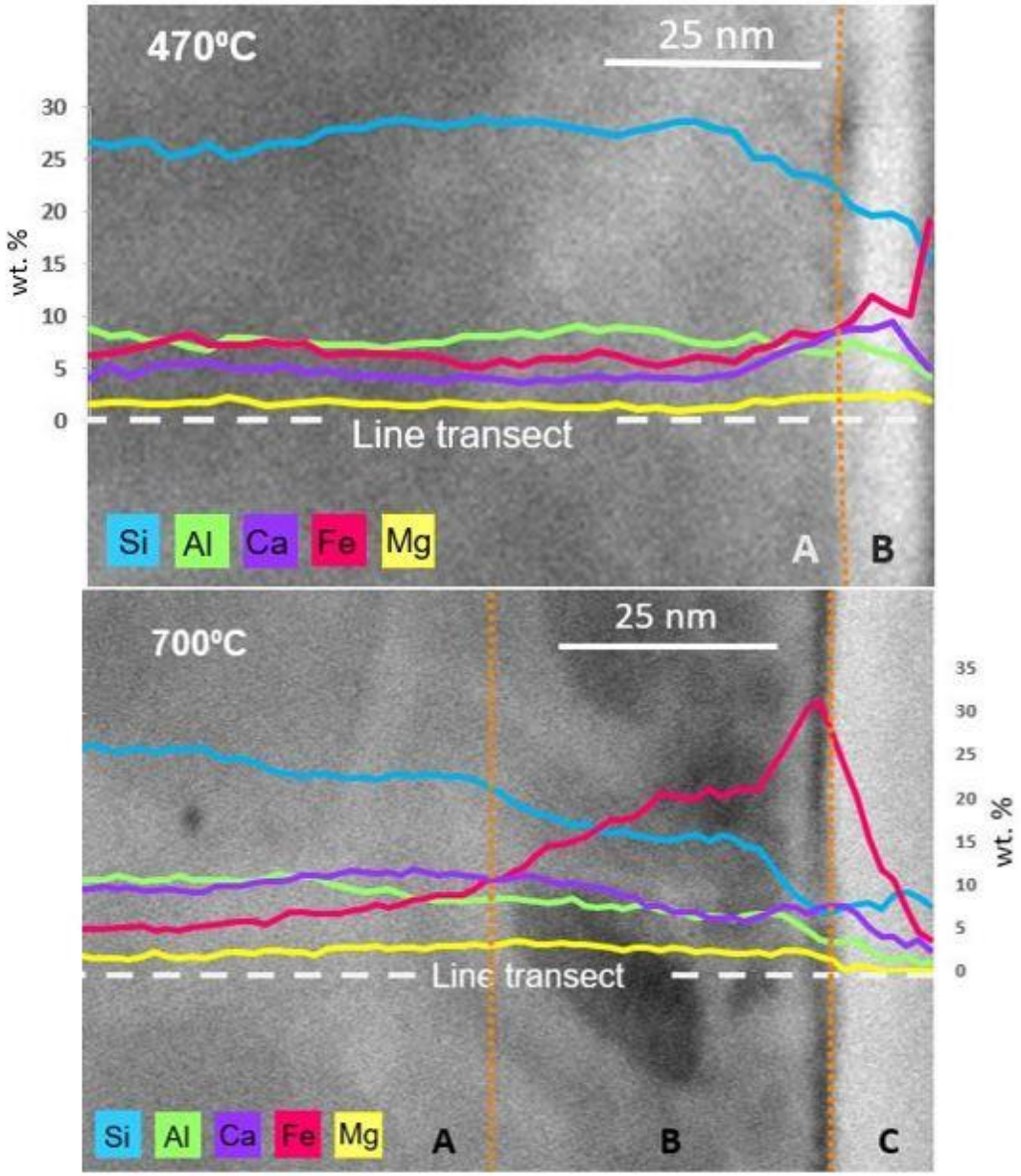

Figure 21. Side-by-side comparison of samples with the same initial starting composition (alkaline basalt) subjected to the same oxygen fugacity, pressure, and time conditions but differing temperature conditions. Sample on the top (VEN-5A) was subjected to surface temperatures (470ºC) and sample on the bottom (VEN-4A) was subjected to a higher temperature than that expected at the surface in order to account for some amount of geologic time (700ºC). Note the different scales on the vertical axes.

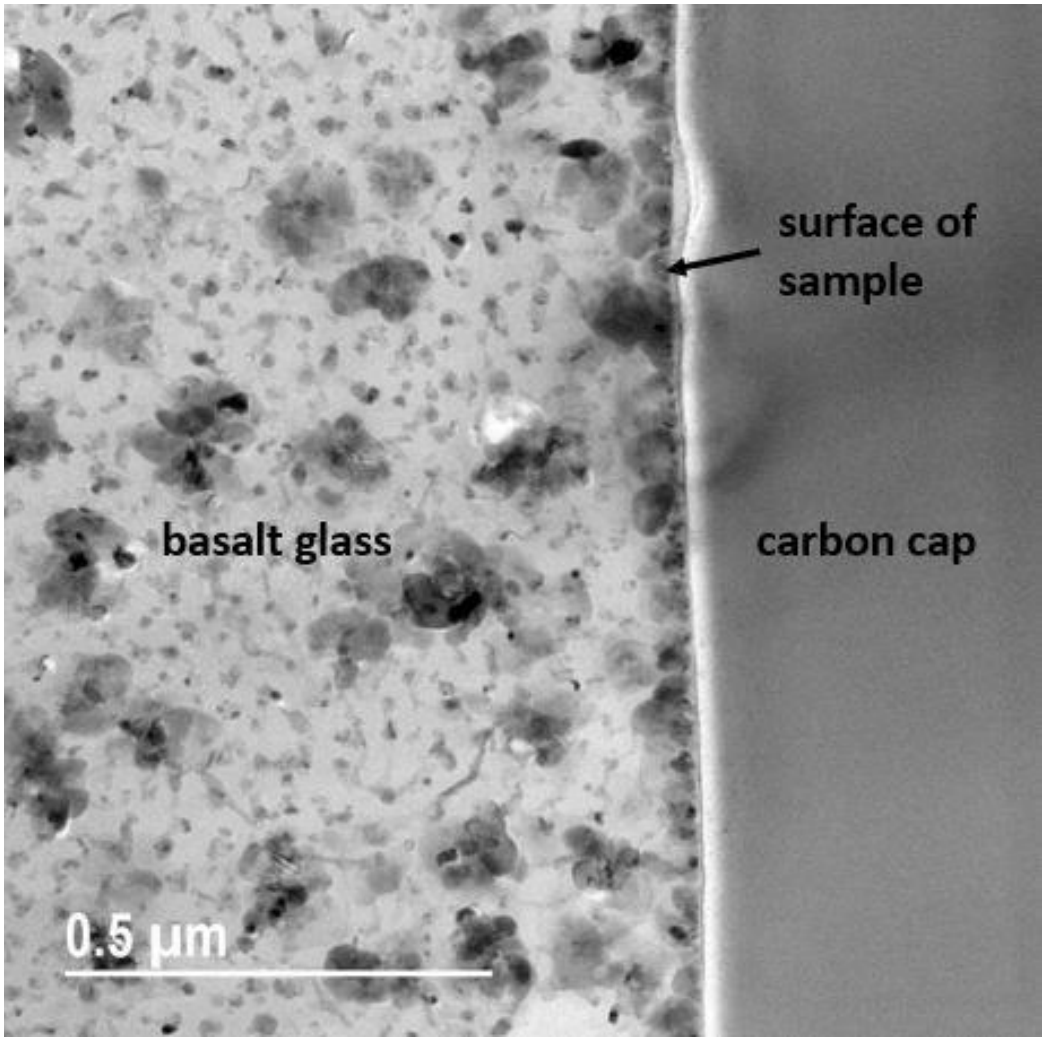

Figure 22. Bright field TEM image (Z-contrast) of sample VEN-4A showing devitrification texture. Darker spots within the basalt glass are nano- to micro-crystalline phases of olivine, pyroxene, and/or ilmenite surrounded by a matrix of feldspathic glass. The phases of olivine and/or pyroxene are present along the surface of the glass where the sample was in contact with the atmosphere during experimentation.

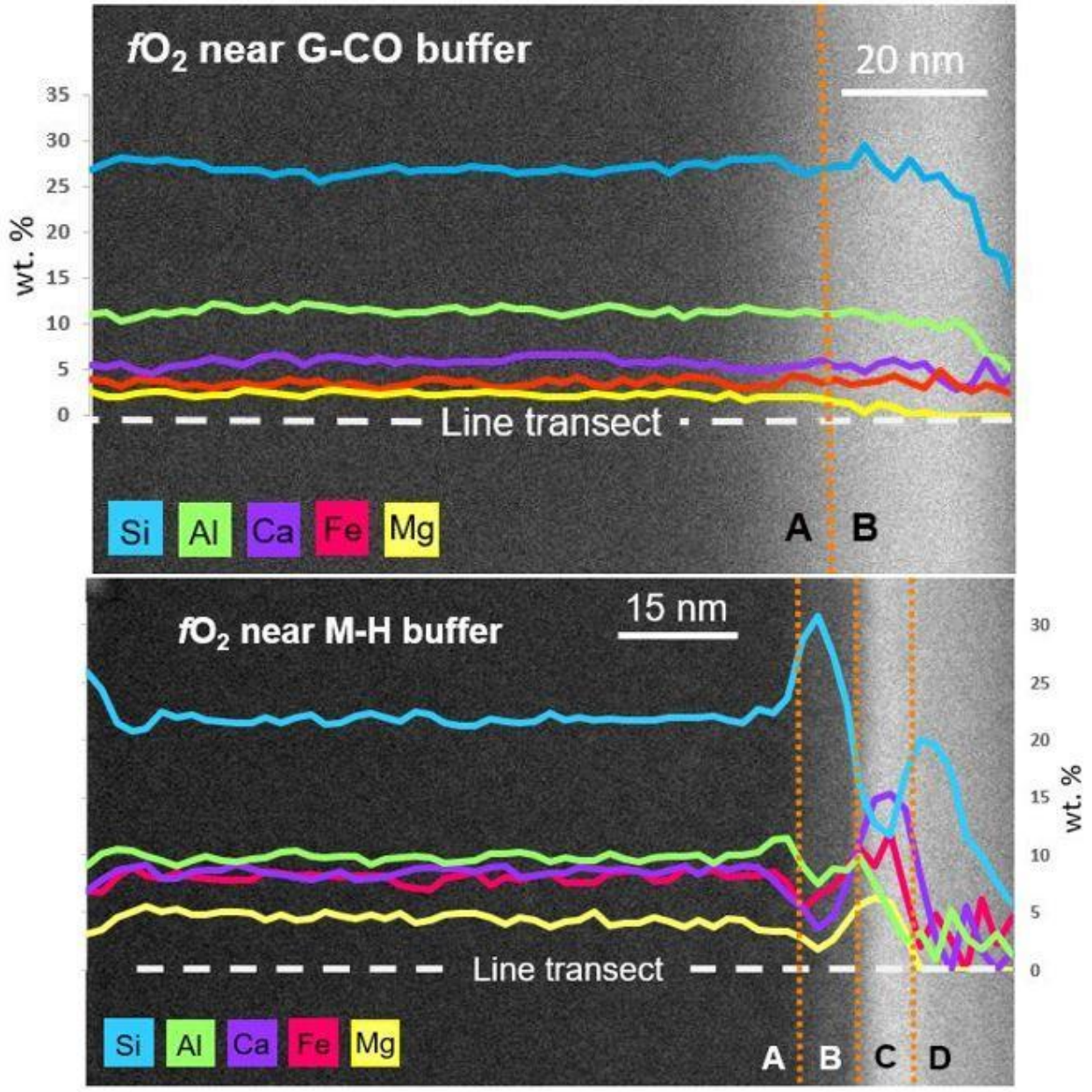

Figure 23. Side-by-side comparison of samples with the same initial starting composition (tholeiitic basalt) subjected to the same pressure, temperature, and time conditions but differing oxygen fugacities. Sample on the top (VEN-1) was subjected to a more reducing atmosphere and the sample on the bottom (VEN-5B) was subjected to a more oxidizing atmosphere. Note the different scales on the vertical axes.

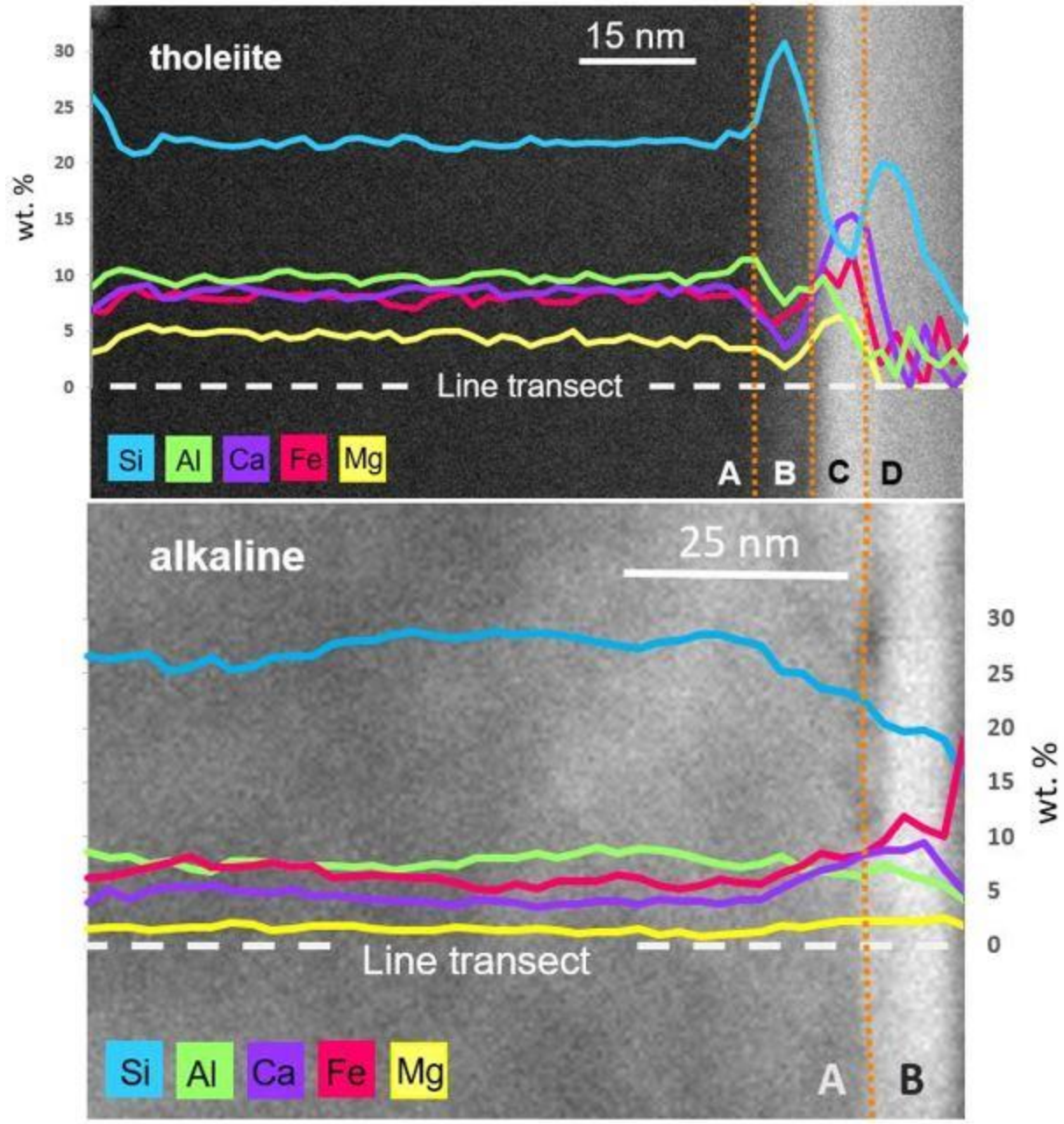

Figure 24. Side-by-side comparison of samples with the same experimentation pressure (90 bars), temperature (470ºC), time (14 days), and oxidation conditions (M-H buffer) but differing starting compositions. Sample on the left (VEN-5B) was a tholeiitic basalt glass and the sample on the right (VEN-5A) was an alkaline basalt glass. Note the difference in appearance of VEN-5A versus VEN-5B is that region C on VEN-5A (left) is a magnetite grain rather than the carbon cap of the sample.

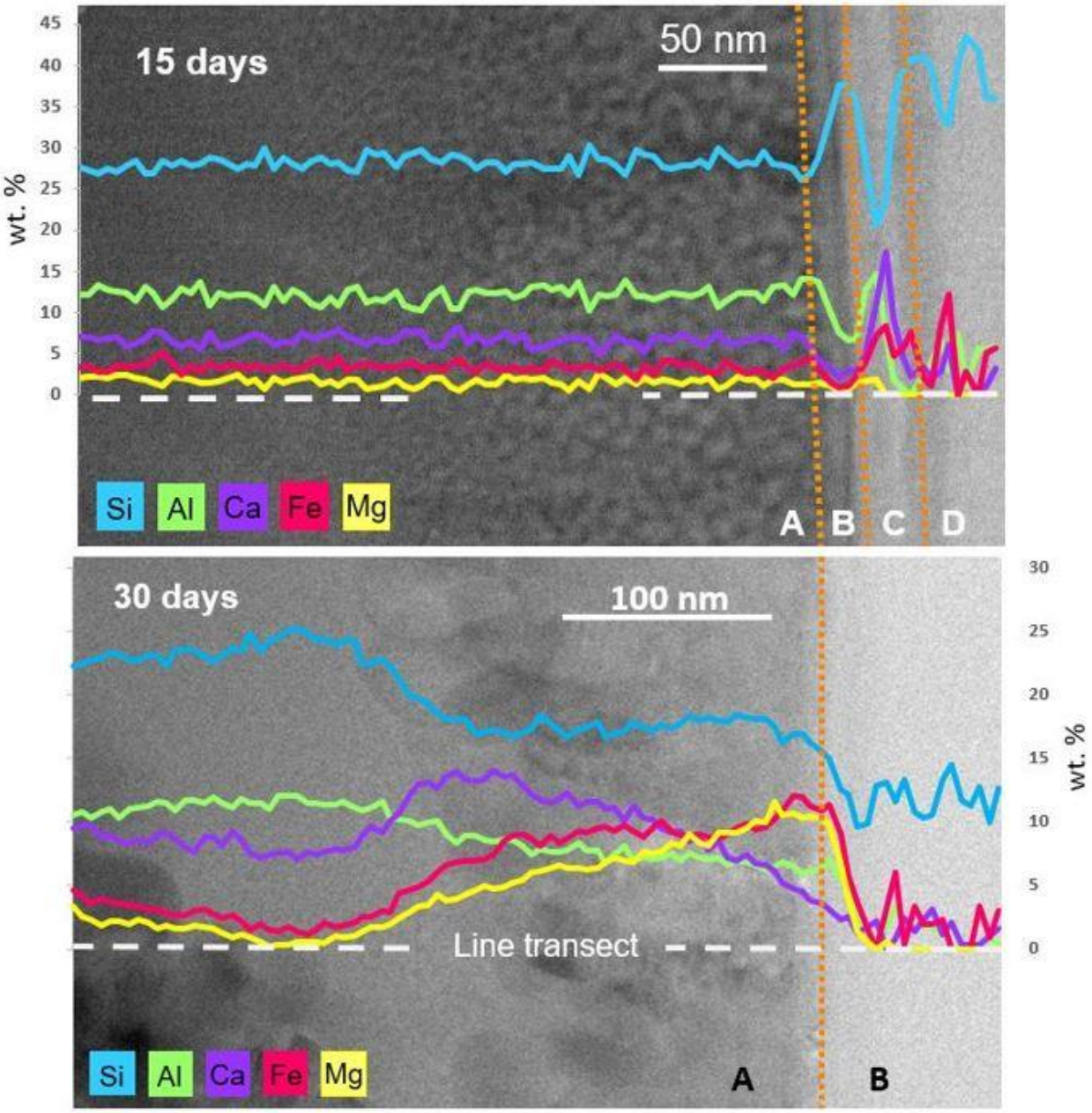

Figure 25. Side-by-side comparison of samples with the same reaction pressure (90 bars), temperature (700ºC), starting composition (tholeiitic basalt), and oxidation conditions (M-H buffer) but differing experimentation durations (15 days versus 30 days). Sample on the left (VEN-4B) was reacted for 15 days and the sample on the right (VEN-7B) was reacted for 30 days.

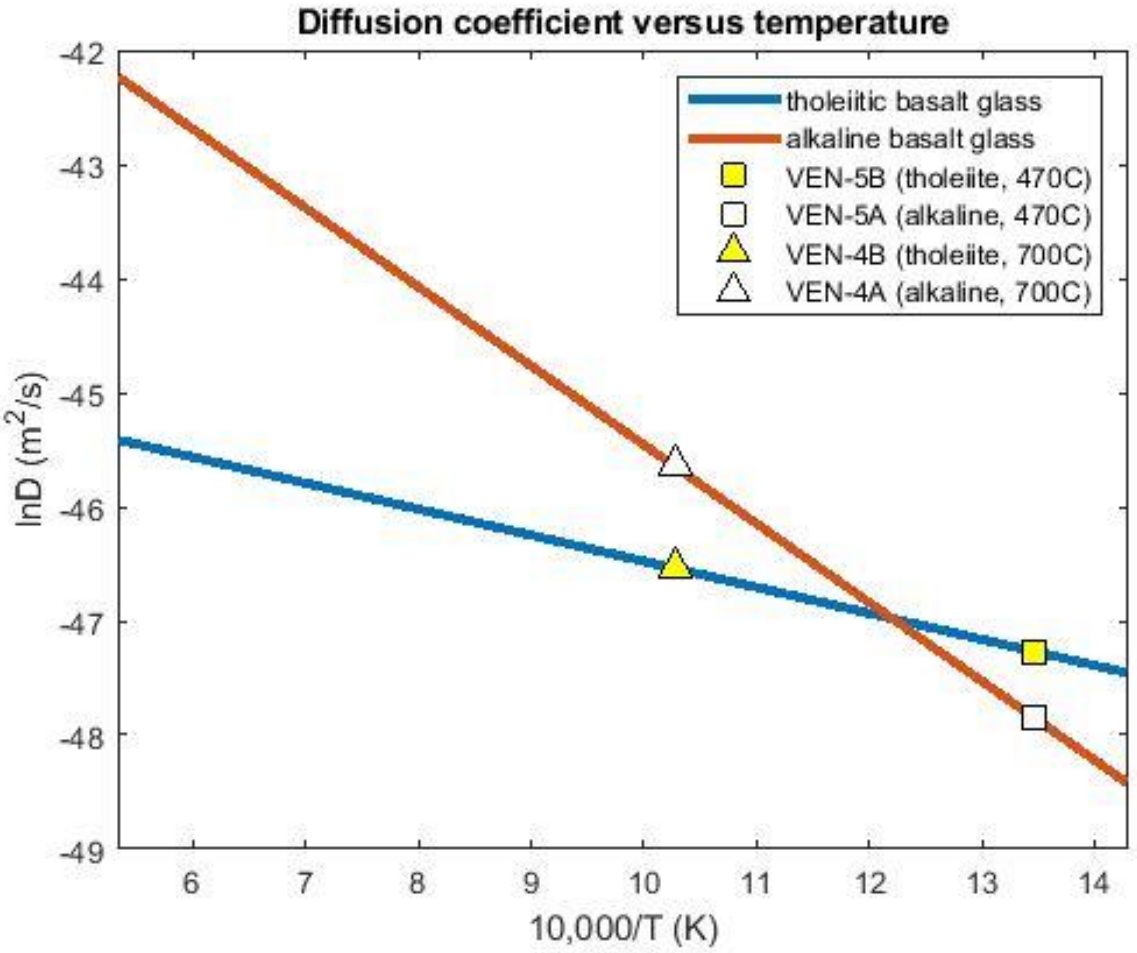

Figure 26. Diffusivity of both tholeiitic and alkaline basalt types versus temperature ranging from 700 K to 1873 K (426ºC to 1600ºC), plotted as 10,000 K. The Arrhenius relation maintains that the slope of the fit is equal to Ea/R and the intercept is equal to lnD. Data points from this study are marked on the respective lines.

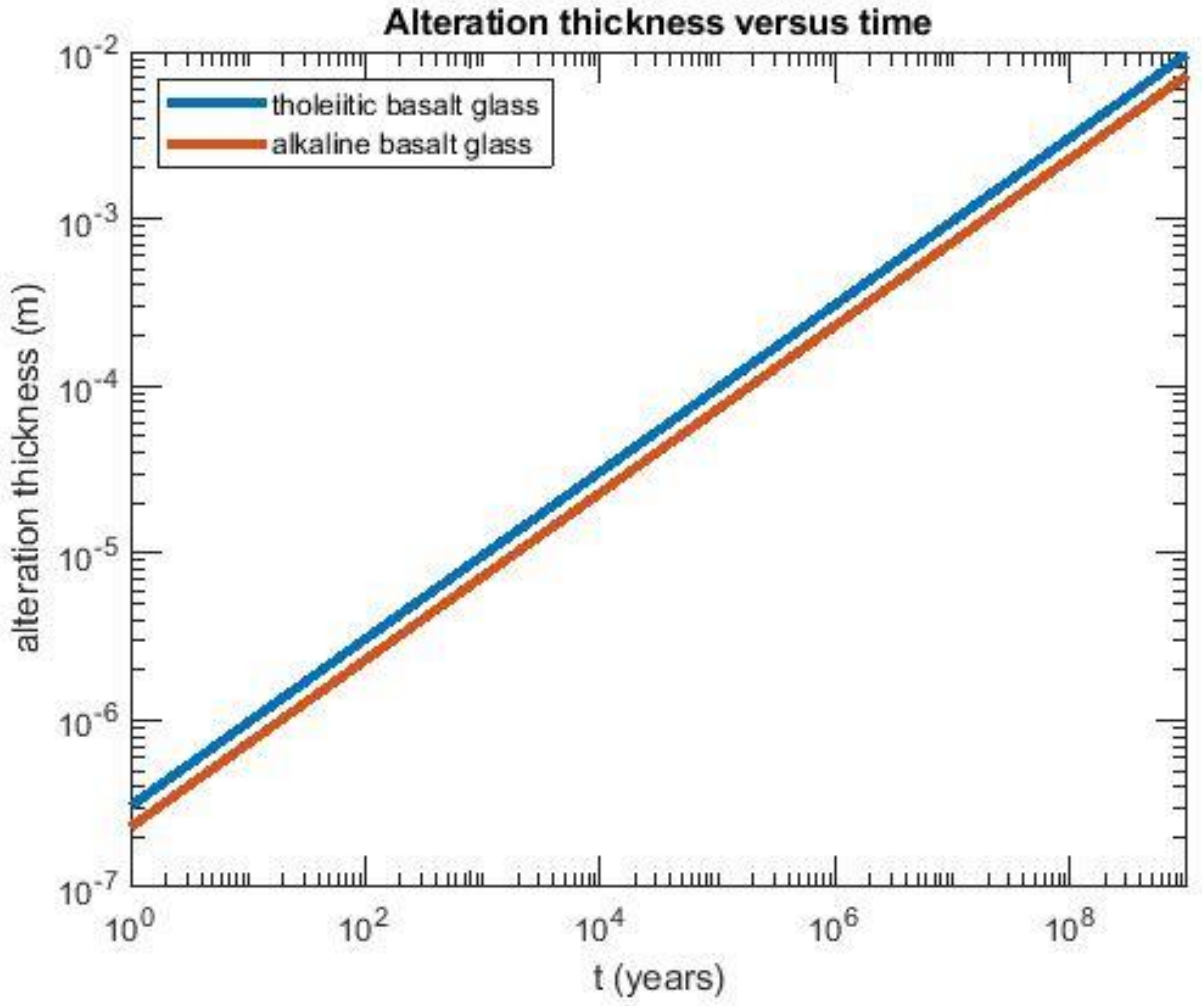

Figure 27. Thickness of alteration rind (in meters) versus time (in years) showing how thick an alteration rind is expected to be over geologic timescales if diffusion is continuous.

Vita

Hannah Teffeteller graduated from the University of Tennessee with a Bachelor of Science degree in geology on August 11th, 2018. She was a first-generation college graduate. During her time as an undergraduate student she received several departmental awards, including the Professor James G. Walls Geology Scholarship, the Otto Kopp Scholarship, the Gordon Award for Professional Promise, the Travis Paris Undergraduate Award, and the Don Byerly Field Camp Scholarship. Ms. Teffeteller went on to pursue her Master of Science degree at the University of Tennessee Department of Earth and Planetary Sciences where she studied the alteration of basalt on the surface of Venus under advisor Dr. Molly McCanta. As a graduate student, she was awarded the GEOL596 Colloquium Presentation Award. She conducted research with colleagues at NASA's Johnson Space Center and presented the group's findings at several national conferences, including the Lunar Planetary and Science Conference and the American Geophysical Union's annual conference.